


# Optical properties of atmospheric particles over an urban site in Mexico City and a peri-urban site in Queretaro

Rafael N. Liñán-Abanto<sup>1,2,3</sup> · O. Peralta<sup>1</sup> · D. Salcedo<sup>4</sup> · L. G. Ruiz-Suárez<sup>1</sup> · P. Arnott<sup>5</sup> · G. Paredes-Miranda<sup>5</sup> · H. Alvarez-Ospina<sup>1,6</sup> · T. Castro<sup>1</sup> 

Received: 7 February 2019 / Accepted: 6 June 2019  
© Springer Nature B.V. 2019

## Abstract

Optical properties of atmospheric particles at Mexico City (UNAM) and Queretaro (JQRO) were measured with a Photoacoustic Extinctionmeter (PAX) at 870 nm. The Mexico City Metropolitan Area has around 21 million inhabitants and Queretaro Metropolitan Area has little more than a million. Observations of meteorological parameters (relative humidity, solar radiation, and wind speed) were used to identify the rainy and dry seasons and explain the daily and seasonal behaviors of particles optical properties. The measurements were made from November 1, 2014 to July 31, 2016. At UNAM, the mean values of the scattering coefficient ( $B_{\text{scat}}$ ) in cold dry, warm dry, and rainy seasons were 35.8, 27.1, and 31.3  $\text{Mm}^{-1}$ , respectively; while at JQRO were 10.9, 11.9, and 15.0  $\text{Mm}^{-1}$ . The average values of the absorption coefficient ( $B_{\text{abs}}$ ) at UNAM during the cold dry, warm dry, and rainy seasons were 14.5, 12.7, and 12.7  $\text{Mm}^{-1}$ , respectively; whereas at JQRO were 4.9, 4.7, and 3.9  $\text{Mm}^{-1}$ . Both absorption and scattering coefficients showed similar diurnal behaviors, but at UNAM they are three times higher than JQRO. Concentrations of criteria gases ( $\text{O}_3$ , NO,  $\text{NO}_2$  and  $\text{NO}_x$ ) were also measured. At UNAM no difference was observed between the seasonal values for the single scattering albedo (SSA); while in JQRO, the rainy season had the highest seasonal value, being 13% higher than in the dry seasons. The Mass Scattering Cross-Section (MSC) values at UNAM were close to 2  $\text{m}^2/\text{g}$ ; on the other hand, at JQRO the MSC values were lower than 1  $\text{m}^2/\text{g}$ . The results suggest a seasonal variability in the aerosol optical properties in both sites, which should be verified with more long-term studies.

**Keywords** Scattering coefficient · Absorption coefficient ·  $\text{O}_3$ - $\text{NO}_x$  relationship · Mass-specific scattering cross section · Single scattering albedo · And  $\text{PM}_{2.5}$

---

✉ T. Castro  
telma@atmosfera.unam.mx

## 1 Introduction

Atmospheric aerosols have gained a lot of attention because of their complex role in atmospheric processes: (a) they directly affect the radiative balance of earth and climate by means of scattering and absorption of incident solar radiation (He et al. 2009; Lyamani et al. 2010), (b) they indirectly impact climate acting as cloud condensation nuclei, thereby changing their microphysical properties (Kaufman et al. 2005; Foster et al. 2007), (c) they affect the concentration of other atmospheric constituents such as ozone (Schwartz et al. 1995) (d) they have impacts on human health (Dockery and Pope 1996; Pope III and Dockery 2006; Borja-Aburto et al. 1998); and (e) they reduce visibility (Horvath 1995; IPCC 2013). Certain atmospheric aerosols, specifically carbonaceous particles and mineral dust, absorb solar radiation which causes an increase in air temperature.

Aerosols optical properties (scattering and absorption coefficients) depend on their size, chemical composition through the refractive index, and mixing state. Aerosols can change their physical, chemical and optical properties due to an increase in water content (Hennigan et al. 2008a, b; Flores et al. 2012; IPCC 2013). Aerosols that strongly contribute to the scattering coefficient include organic particles, water-soluble inorganic species (sulfates, nitrates and ammonium), dust, and sea salt (Lyamani et al. 2010).

The temporal and spatial distribution of aerosols in the planetary atmosphere is very variable. It is estimated that the residence time in the atmosphere varies from less than one day to more than one month, resulting in transport distances of a few miles to hemispheric scales (Marley 2000; Williams et al. 2002). This variability in composition and distribution makes it difficult to quantify the impact of aerosols on climate.

Aerosol models have suggested that scattering and absorption could cause changes in the surface of UV radiation field (Corr et al. 2009; Liu et al. 1991). These aerosol disturbances in the field of UV radiation can lead to substantial changes in tropospheric photolytic reaction rates (Castro et al. 1997), which may influence VOC photo-oxidation pathways. These changes are complex and depend on the altitude, chemical regime and scattering or absorption of aerosols.

Understanding the absorption of solar radiation by atmospheric particles (i.e. black carbon, BC) is important to explain the effects of particles on climate. Particles with low absorption capacity have a negative climate forcing (cooling) while particles with high absorption can have a positive forcing (warming) (Heintzenberg et al. 1997). BC particles have received more interest since results were published indicating that it may be cheaper to control black carbon particles than CO<sub>2</sub> (Hansen et al. 2000). The reduction of BC emissions represents a potential mitigation strategy that could reduce the global climatic forcing of anthropogenic activities in the short term (Bond et al. 2013).

In climate models it is important to represent the optical properties of atmospheric aerosols. It is assumed that their radiative effects can be predicted from their concentrations and chemical composition. Predicting this relationship is a major challenge, because scattering and absorption depend on the shape of the particles (Bond and Bergstrom 2006).

Air pollution is a global problem in areas where volatile organic compounds (VOC's) and NO<sub>x</sub> emissions from the main mobile and stationary sources are "trapped" by thermal inversions and irradiated by sunlight during transport to regions downwind (Finlayson and Pitts, 2000). Particles are not the only ones that age in the photochemical aerosol, other reactive chemical species change their concentrations and the ratios between them in such a way that some of these ratios can be used as a photochemical indicator (PI) of the age of the aerosol. The ratio O<sub>3</sub>/NO<sub>y</sub> is one of those (Chameides et al. 1994; Zaveri et al. 2003; Sillman

and He 2002). In general, in a plane ( $\text{NO}_y$ ,  $\text{O}_3$ ), low  $\text{O}_3$  with high  $\text{NO}_y = \text{NO}_x + \text{NO}_z$ , concentrations, along the X axis, correspond to VOC sensitive conditions. These conditions may also indicate photochemically young air parcels, when most of  $\text{NO}_y$  is still in the form of  $\text{NO}_x = \text{NO} + \text{NO}_2$ . On the other hand, high  $\text{O}_3$  and low  $\text{NO}_y$  concentrations, along the Y axis, correspond to  $\text{NO}_x$  sensitive conditions. These conditions also indicate aged parcels where most of  $\text{NO}_y$  is in the form of  $\text{NO}_z = \text{HNO}_3 + \text{PAN} + \text{RONO}_2$  like species. It has been shown that current standard  $\text{NO}_x$  monitors (Dunlea et al. 2007) suffer the positive artifact of being sensitive to some  $\text{NO}_z$  compounds. The positive interference increases along the day. From this fact, in the absence of  $\text{NO}_y$  instruments, afternoon (12:00 to 15:00)  $\text{NO}_x^*$  measurements have been taken as surrogates of  $\text{NO}_y$  (García-Yee et al. 2018).

In this paper we present optical properties results of particles and criteria pollutants, measured at two Mexican cities (urban and peri-urban), from November 2014 to July 2016. Meteorological parameters (wind speed, relative humidity and solar radiation) are also analyzed. The seasonal and diurnal variations of the optical properties and criteria pollutants are explained from the anthropogenic activities and meteorology. The main objective of this study is to evaluate the temporal variations of the optical properties and the criteria pollutants in the two sites; and analyze how they are influenced by the seasonal variations of the meteorological parameters. Our results suggest a seasonal variability of aerosols and remarks the importance of long-term studies. This study exposes the little knowledge that exists regarding chemical and physical processes occurring under different atmospheric conditions in a Megacity (Mexico City) and Queretaro, a medium size city with a strong socioeconomic growth. Queretaro is important not because it is a medium size city of Mexico, but it represents what Mexico City could have been 20 years ago when it was under a  $\text{NO}_x$  sensitive regime. In short time, many medium-large cities such as Bogota, Lima, Buenos Aires, Jakarta, Tianjin, Dhaka, and many others around the world will undoubtedly grow and live under a VOC sensitive regime, undergoing modifications in the particles chemical composition and optical properties, modifying the radiative budget of the atmosphere.

## 2 Experimental

The measurements of optical properties and gaseous pollutants presented in this study were collected in an urban site in Mexico City and a peri-urban site in Queretaro, from November 1, 2014 to July 31, 2016. Additionally, meteorological parameters (wind speed, relative humidity, solar radiation, and precipitation) were also measured. Since we were looking the seasonal trends, the measurements period was sorted as follows, based on the annual periodicity: cold dry season (November 2014 to February 2015, and November 2015 to February 2016), warm dry season (March to April 2015, and March to April 2016), and rainy season (May to October 2015 and May to July 2016).

### 2.1 Measurement sites

#### 2.1.1 Mexico City site (UNAM)

The UNAM-RUOA observatory at Mexico City is on the roof of the Centro de Ciencias de la Atmósfera (Atmospheric Sciences Center, CCA) building at UNAM campus, in the southeast quadrant of Mexico City ( $19^\circ 19' 34''$  N,  $99^\circ 10' 34''$  W, 2280 m above sea level) (Fig. 1). Air

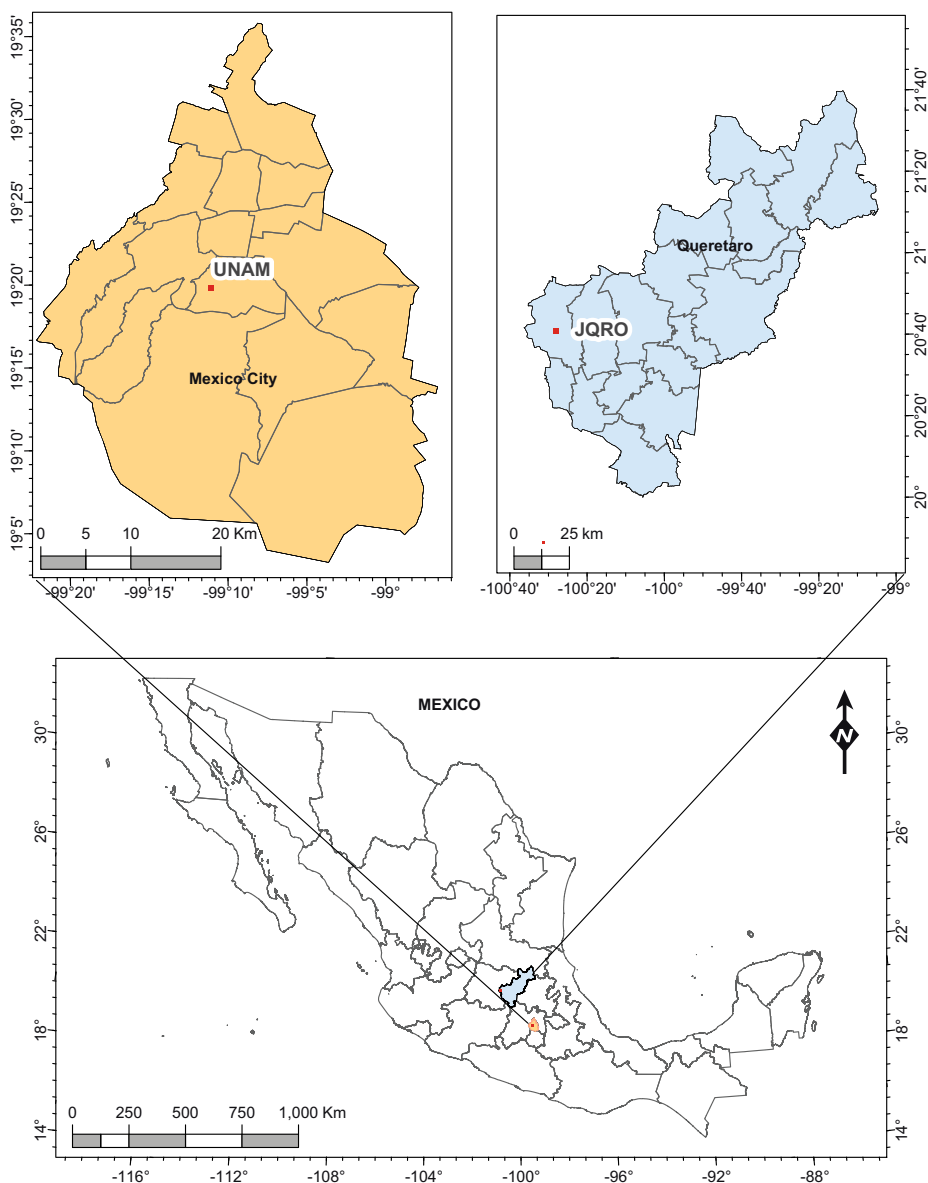


**Fig. 1** Location of the UNAM and JQRO observatories of the Red Universitaria de Observatorios Atmosféricos (University Network of Atmospheric Observatories, RUOA) in Mexico City and Juriquilla- Queretaro, respectively

samples were taken approximately 15 m above ground level (m.a.g.l). The campus is located within a residential area with very little industrial activity; however, there is vehicular traffic nearby. The site is about 400 m to the northwest of a subway station, and there are many public transport buses in its surroundings (Peralta et al. 2007).

Mexico City has a sub-tropical climate, and three climatic seasons have been identified: cold dry (November–February); warm dry (March–April) and rainy (May–October) ((Jáuregui 1973; Ruiz Suárez et al. 1999; De Foy et al. 2005; Bravo et al. 2014). Climate throughout the year is determined



by two major regional alternating currents: the predominantly dry western winds that extend over Mexico during the dry season from November to April associated with dry conditions and light winds (anticyclonic climate); and the humid northeast wind current that brings the rains from May to October (Jáuregui 1973, 1997, 2002). These weather and climate patterns have an important influence on the behavior and distribution of pollution throughout the year (Castro et al. 1997).

### 2.1.2 Queretaro site (JQRO)

The JQRO-RUOA observatory is in the UNAM campus in Juriquilla, located in the northern limit of Queretaro Metropolitan Area (20°42'11" N 100°26'50" W, 1893 m.a.s.l.) (Fig. 1). Air inlets were located approximately 15 m.a.g.l. This campus is surrounded by residential and commercial areas, which are adjacent to a highway with mixed traffic.

Queretaro has 1.2 million inhabitants (approximately 45% of the state's population) and is located 220 km to the northwest of Mexico City. Its predominant climate is semi-dry temperate, with a temperature range of 12 to 20 °C, and rainfall between 500 to 700 mm (INEGI 2018). Two of the major highways in Mexico, Route 45 and Route 57, connect the northwest and northeast of Mexico through Queretaro (Burgos and Johnson 2016).

## 2.2 Measurement methods

### 2.2.1 Meteorological parameters

The meteorological parameters (relative humidity, solar irradiance and wind speed) at UNAM and JQRO observatories were measured with a time resolution of 1 min. Precipitation was measured with a Lufft Model WS600-UMB Doppler radar with a response limit of 0.002 mm. The relative humidity was measured with a Lufft Model WS600-UMB device, which measures the difference in the conductive capacity of a polymer film sensor at humidity changes with a sensitivity of 3%. The wind speed (intensity and direction) was measured with a Lufft Model WS600-UMB ultrasonic anemometer with three transducers in horizontal plane (minimum activation limit 0.3 m/s and accuracy <3°).

### 2.2.2 Criteria pollutants

Criteria gases ( $O_3$ , NO,  $NO_2$  and  $NO_x$ ) and particles ( $PM_{2.5}$ ) concentrations were measured with a time resolution of 1 min. Ozone concentration at UNAM observatory was measured with an ozone analyzer Teledyne API T400; while in JQRO, it was measured with a Thermo Scientific model 49i. Both analyzers use UV absorption photometry technology, with a lower detection limit of 0.03 ppb.

At UNAM, nitrogen oxides (NO,  $NO_2$  and  $NO_x$ ) were measured with a NO- $NO_2$ - $NO_x$  analyzer Teledyne API 200E using Chemiluminescence technology, with a lower detectable limit 0.40 ppb. In JQRO, a NO- $NO_2$ - $NO_x$  analyzer Thermo Scientific 42i with a lower detectable limit 0.40 ppb (60 s averaging time) was used.

At UNAM,  $PM_{2.5}$  concentration was measured with C14 FH62C14 Continuous Ambient Particulate Monitor (FH62C14) from Thermo Andersen BAM; while at JQRO a Thermo Scientific FH62C1410, which is a radiometric particulate mass monitor capable of providing real-time measurements, was used. The FH62C14 monitor incorporates time-averaged measurements of an integral beta attenuation mass sensor. An EPA head is used for size separation, the lower limit of detection is <4  $\mu\text{g}/\text{m}^3$  for averages of one hour.

### 2.2.3 Optical properties

Light absorption and scattering coefficients of particles with an aerodynamic diameter smaller than 2.5  $\mu\text{m}$  were measured in situ using a photoacoustic extinctionsmeter (PAX, DMT Inc.). This instrument performs simultaneous measurements of the scattering coefficient ( $B_{\text{scat}}$ ) and absorption coefficient ( $B_{\text{abs}}$ ) of aerosols, and based on these coefficients, derives the single scattering albedo (SSA) and the black carbon (BC) mass concentration. It uses a laser diode modulated at 1500 Hz and at 870 nm. This standard infrared wavelength is highly specific for black carbon particles. A nominal flow of aerosol samples of 1 L/min passes through the PAX using an internal vacuum pump controlled by two critical orifices. The flow is divided between the nephelometer and a photoacoustic resonator for simultaneous measurements of the scattering and absorption coefficients, respectively. Absorption measurements use photoacoustic technology (Arnott et al. 1999, 2000). A laser beam directed through the aerosol stream is modulated at the resonance frequency of the acoustic chamber. Absorbent particles heat up and quickly transfer heat to the surrounding air. Periodic heating produces pressure waves that can be detected with a sensitive microphone. The absorption coefficient is directly proportional to the pressure detected by the microphone. The nephelometer measures the scattering coefficient. Light scattering and absorption by particles depend on its chemical composition, the mixing state and morphology (Arnott et al. 1999; Paredes-Miranda et al. 2009; Retama et al. 2015).

## 3 Results and discussion

For the analysis of the temporal variations of optical properties ( $B_{\text{scat}}$ ,  $B_{\text{abs}}$ , and SSA), criteria pollutants ( $\text{PM}_{2.5}$ ,  $\text{O}_3$ ,  $\text{NO}$ ,  $\text{NO}_2$ , and  $\text{NO}_x$ ), and meteorological parameters (precipitation, relative humidity, solar irradiance and wind speed), hourly values were obtained by averaging the recorded measurements. Subsequently, the data was grouped into seasons (cold dry, warm dry and rainy) for the full study period. The statistics of meteorological parameters, criteria pollutants, and optical properties are shown in Tables 1, 2 and 3, respectively.

**Table 1** Seasonal statistics of meteorological parameters at UNAM (Mexico City) and JQRO (Juriquilla-Queretaro)

Meteorological parameters	Statistic	UNAM				JQRO			
		Cold dry	Warm dry	Rainy	Full Period	Cold dry	Warm dry	Rainy	Full Period
Relative humidity (%)	Minimum	6	8	11	6	6	4	7	4
	Media	53	48	64	57	55	47	63	57
	Maximum	96	94	96	96	99	97	99	99
Solar irradiance ( $\text{W}/\text{m}^2$ )	Minimum	0	0	0	0	0	0	0	0
	Media	176	255	217	208	206	267	261	241
	Maximum	979	1136	1116	1136	1000	1132	1154	1154
Wind speed (m/s)	Minimum	0.3	0.3	0.3	0.3	0.3	0.3	0.3	0.3
	Media	1.3	1.6	1.4	1.4	2.7	2.7	2.5	2.6
	Maximum	6.4	8.2	5.7	8.2	9.0	11.6	10.1	11.6

**Table 2** Seasonal statistics of criteria pollutants at UNAM (Mexico City) and JQRO (Juriquilla-Queretaro)

Criteria pollutants	Statistic	UNAM				JQRO			
		Cold dry	Warm dry	Rainy	Full Period	Cold dry	Warm dry	Rainy	Full Period
O <sub>3</sub> (ppb)	Minimum	1.0	1.0	1.0	1.0	0.3	0.4	0.3	0.3
	Average	26.4	35.0	34.0	31.4	27.3	35.8	32.8	31.4
	Maximum	135.5	164.0	171.0	171.0	85.4	94.0	104.2	104.
NO <sub>x</sub> (ppb)	Minimum	4.2	4.0	4.0	4.0	0.4	0.4	0.4	0.4
	Average	52.2	38.2	35.2	42.6	20.7	18.3	13.2	17.6
	Maximum	267.5	248.0	288.0	288.0	317.4	160.6	140.6	317.4
PM <sub>2.5</sub> (μg/m <sup>3</sup> )	Minimum	1.0	1.0	1.0	1.0	1.0	1.0	1.0	1.0
	Average	21.0	19.1	16.6	18.8	12.3	13.5	13.1	12.9
	Maximum	302.0	104.0	74.0	302.0	81.5	51.4	57.1	81.5

### 3.1 Meteorological measurements

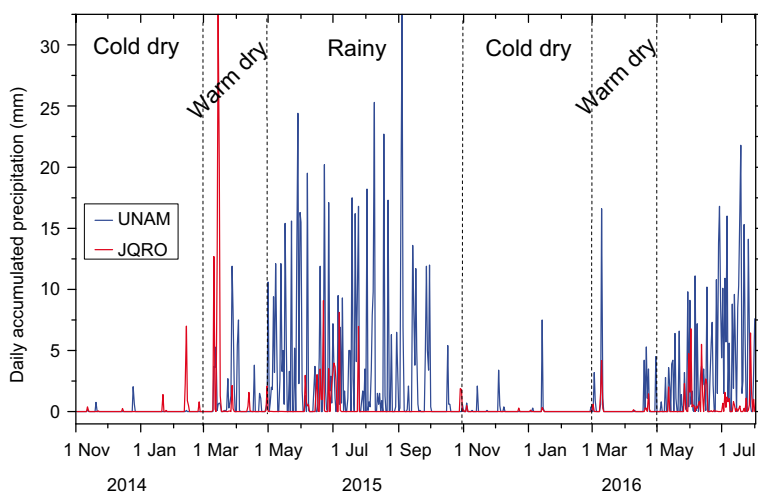
Figure 2 shows the time series of the daily accumulated precipitation at UNAM and JQRO, during the entire study period. In Mexico City, rain episodes occur from May to October, while in JQRO from June to July with sporadic rainfall in other seasons. Data shown in Fig. 2 were used to determine the different seasons during the entire study period (21 months), which roughly coincide with the seasons proposed by de Foy et al. (2005).

Table 1 shows the seasonal statistics of relative humidity, solar irradiance and wind speed at the two measuring sites. In both places the relative humidity increases during the rainy season and decreases in the warm dry season, the highest average values of solar irradiance and wind speed occur in the warm dry season.

Figure 3 (a–f) show the seasonal daily cycles of relative humidity, solar irradiance and wind speed, at UNAM and JQRO during the entire period of measurements. At UNAM, the daily cycle of relative humidity shows a maximum (06:00–07:00 LT) and a minimum (15:00–16:00 LT) during all seasons (Fig. 3a). Similar daily pattern of relative humidity is observed in JQRO, its maximum value is given at 07:00–08:00 LT and its minimum value around 15:00–16:00 LT during the three seasons

**Table 3** Seasonal statistics of optical properties of particles at UNAM (Mexico City) and JQRO (Juriquilla-Queretaro)

Optical properties	Statistics	UNAM				JQRO			
		Cold dry	Warm dry	Rainy	Full Period	Cold dry	Warm dry	Rainy	Full Period
B <sub>scat</sub> (Mm <sup>-1</sup> )	Minimum	1.0	1.1	1.2	1.0	0.1	0.2	0.8	0.1
	Average	35.8	27.1	31.3	31.9	10.9	11.9	15.0	12.9
	Maximum	679.9	157.1	272.0	679.9	74.3	92.1	88.6	92.1
B <sub>abs</sub> (Mm <sup>-1</sup> )	Minimum	0.7	1.1	1.2	0.7	0.1	0.3	0.4	0.1
	Average	14.5	12.7	12.7	13.3	4.9	4.7	3.9	4.4
	Maximum	84.0	70.6	75.3	84.0	54.7	32.8	31.0	54.7
SSA	Minimum	0.18	0.13	0.12	0.12	0.17	0.12	0.31	0.12
	Average	0.67	0.66	0.66	0.66	0.69	0.69	0.78	0.73
	Maximum	0.94	0.93	0.96	0.96	0.96	0.95	0.98	0.98



**Fig. 2** Time series of daily accumulated precipitation during the entire study period from November 2014 to July 2016 at UNAM and JQRO sites. The study period covers the seasons: cold dry 2014–2015 and 2015–2016, warm dry 2015 and 2016, and rainy 2015 and 2016

(Fig. 3b). Also, the solar irradiance at both sites (Fig. 3c, d) shows the same pattern during all seasons. It increases from its minimum value early in the morning to a maximum (12:00–13:00 LT). The daily trends of wind speed at UNAM (Fig. 3e) and JQRO (Fig. 3f) show the same pattern too, with the minimum in the morning and the maximum in the afternoon. At UNAM, the minimum value of wind speed is given at 07:00–08:00 LT during the three seasons, and the maximum at 17:00–18:00 LT in the dry seasons, and one hour later in the rainy season. At JQRO, the minimum is at 08:00–09:00 LT during all seasons, while the maximum is reached at 17:00–18:00 LT in dry seasons, and two hours later in the rainy season. During the three seasons, the average daily wind speed is more than 2 m/s (intermediate wind speed), while at UNAM is less than 2 m/s (weak wind speed). In both sites, the highest values of wind speed occur during the warm dry season.

## 3.2 Criteria pollutants

### 3.2.1 Gases

In both sites, the warm dry season has the maximum average of ozone and cold dry season the minimum (Table 2). Also, the cold dry season has the maxima  $\text{NO}_x$  averages concentrations and the rainy season the minima.  $\text{NO}_x$  concentrations at UNAM are more the double than those of JQRO.

Figure 4 (a–f) compares the daily cycles of  $\text{O}_3$ ,  $\text{NO}$  and  $\text{NO}_2$  at UNAM and JQRO during the three seasons. At UNAM the following characteristics are observed: in the early morning the concentration of  $\text{NO}$  increases due to vehicle emissions and reaches its maximum approximately at the maximum density of traffic. At the same time, that  $\text{NO}$  reaches its maximum, the concentration of ozone begins to increase. Subsequently, the  $\text{NO}_2$  reaches its maximum. Ozone levels are relatively low early in the morning (in hours of maximum  $\text{NO}$ ), and increase significantly around noon, when the concentration of  $\text{NO}$  falls to its minimum values. The planetary boundary layer height is likely low in the morning, trapping the pollution, and the wind speed is low at that time, keeping the pollution from being removed. Unlike Mexico City, in JQRO  $\text{NO}_2$  begins to decrease at the same time as  $\text{NO}$  (between 07:00 and 09:00:00 LT, depending on the season).

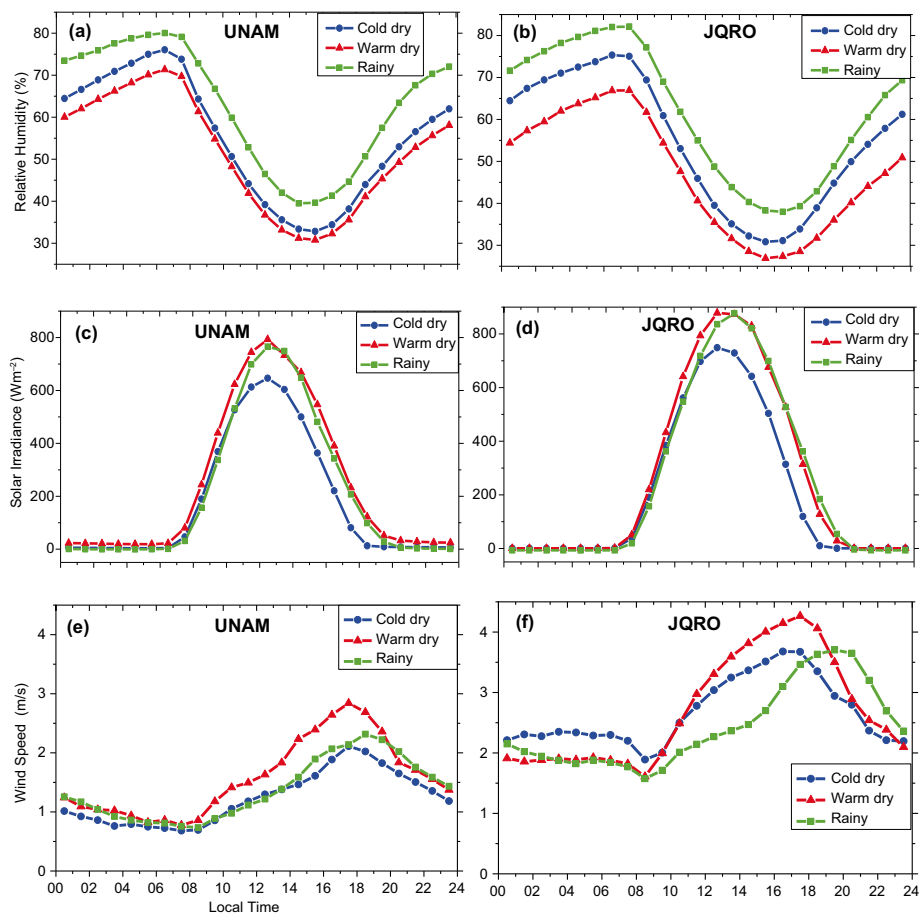


**Fig. 3** Daily patterns of: relative humidity (a, b); solar irradiance (c, d); wind speed (e, f), at UNAM (panels on the left) and JQRO (panels on the right) sites, during the three seasons

We used the morning time when NO and O<sub>3</sub> crossover (i.e.,  $t_{\text{NO}=\text{O}_3}$ ) as an end signal of the inhibition period and the beginning of O<sub>3</sub> production via conversion of NO to NO<sub>2</sub> by peroxy radicals (Fujita et al. 2002). Ozone accumulation was estimated by the difference between time of maximum ozone ( $t_{\text{maxO}_3}$ ) and  $t_{\text{NO}=\text{O}_3}$ . The ozone accumulation rate is calculated as the increase in ozone from  $t_{\text{NO}=\text{O}_3}$  to  $t_{\text{maxO}_3}$  divided by the time of ozone accumulation. In UNAM, the start of the accumulation period occurs between 10:00 and 11:00 LT and lasts for 5 h; while in JQRO, the accumulation time is 7 h and begins at 09:00–10:00 LT. The rate of ozone formation is faster in Mexico City than in JQRO (Fig. 4 (a–f)). In JQRO, nocturnal concentrations of ozone were higher than in Mexico City.

The O<sub>3</sub>/NO<sub>y</sub> ratio is used as a photochemical indicator (PI) to determine the sensitivity of ozone production to NO<sub>x</sub> (photochemically aged air masses) and to VOC (air masses containing fresh emissions of ozone precursors). In Torres-Jardón et al. (2009) a value of 8.1 is proposed for the O<sub>3</sub>/NO<sub>y</sub> ratio (transition range of 7.5–10.0) as the photochemical indicator to determine the sensitivity of ozone production to NO<sub>x</sub> or VOCs in Mexico City.

Salcedo et al. (2012) and García-Yee et al. (2018) have used O<sub>3</sub>-NO<sub>x</sub>\* scatterplots (NO<sub>x</sub>\* is NO<sub>x</sub> measured with a chemiluminescent analyzer and it is used as a surrogate of NO<sub>y</sub>). The NO<sub>x</sub>-limited

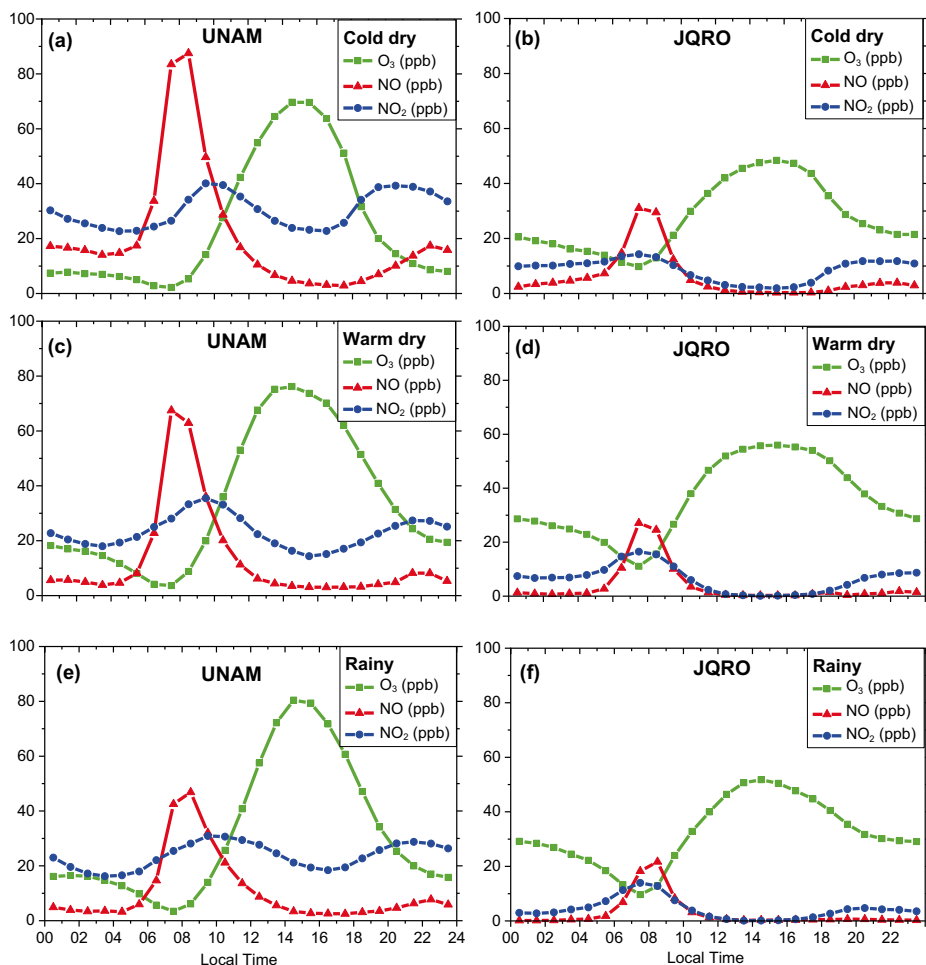


**Fig. 4** Concentration-time profiles of NO, NO<sub>2</sub>, and O<sub>3</sub>, at UNAM (panels on the left) and JQRO (panels on the right) observatories, during the three seasons. The scale is the same for both measurement sites

region is located to the left of the transition range, characterized by relatively high values of O<sub>3</sub>/NO<sub>y</sub> and low NO<sub>y</sub>; while to the right of the transition range it is located, in the VOC-limited region, characterized by high values of NO<sub>y</sub> and low values of O<sub>3</sub>/NO<sub>y</sub>.

Figure 5(a–f) shows the O<sub>3</sub>–NO<sub>x</sub> scatterplots at UNAM and JQRO during the three seasons. At UNAM, the data points fell in the VOC-limited region of the O<sub>3</sub>–NO<sub>x</sub> scatterplots, indicating that ozone production is sensitive to changes in VOC concentrations, suggesting the predominance of air masses with fresh emissions of ozone precursors, while at JQRO, most of the data points fell in NO<sub>x</sub>-limited region, associated with photochemically aged air mass (Torres-Jardón et al. 2009; Salcedo et al. 2012; García-Yee et al. 2018).

### 3.2.2 Particulate matter (PM<sub>2.5</sub>)

Table 2 shows the seasonal statistics of the mass concentration of particulate matter with an aerodynamic diameter smaller than 2.5 μm (PM<sub>2.5</sub>) during the entire period of measurements in

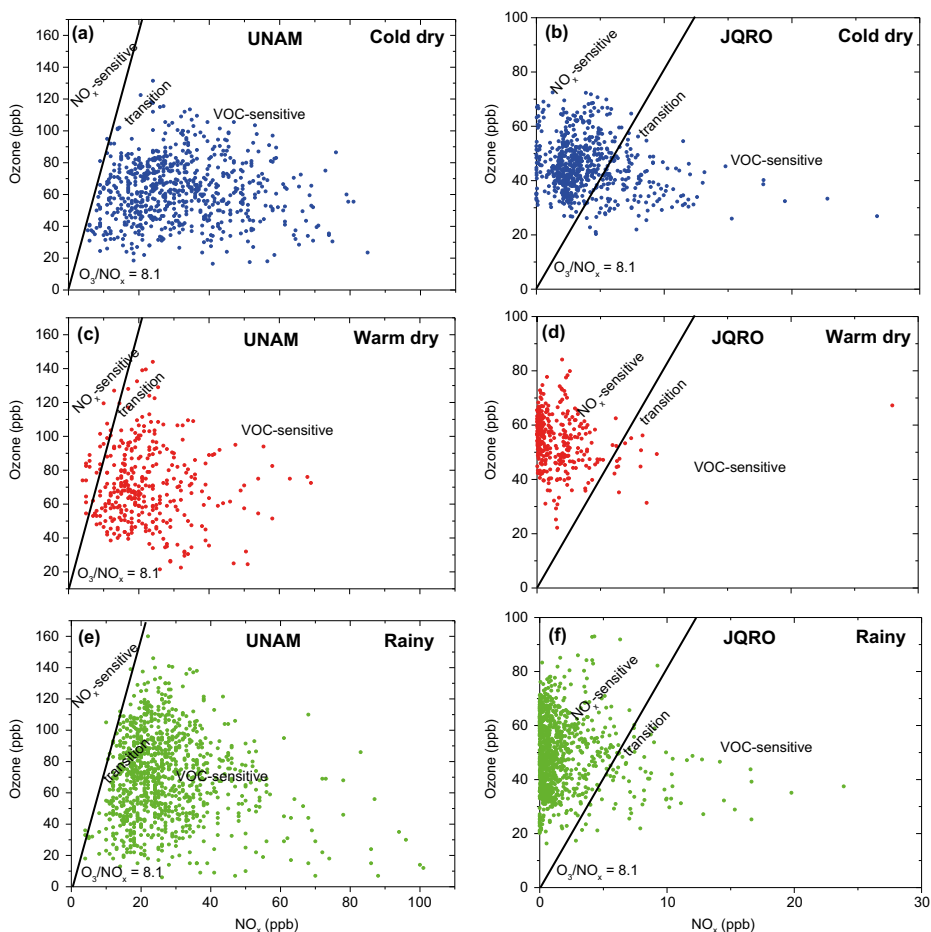


**Fig. 5** Scatterplots of the O<sub>3</sub>-NO<sub>x</sub> concentrations at UNAM and JQRO during the three seasons. The measurements of the concentrations considered were taken between 12:00 and 15:00 LT. In both sites, the O<sub>3</sub> scales are the same, while the NO<sub>x</sub> scales are different

UNAM and JQRO. The seasonal variations of PM<sub>2.5</sub> present differences in the two observatories of the RUOA: in UNAM, the highest value of PM<sub>2.5</sub> mass concentration occurs in the cold dry season and the lowest in the rainy season; in JQRO, the highest value occurs in the warm dry season and the lowest in the cold dry season.

Figure 6 (a-b) shows the daily seasonal cycles of PM<sub>2.5</sub> at UNAM and JQRO, during the entire study period. At UNAM, the daily trends of PM<sub>2.5</sub> in the three seasons are similar; they increase slowly from midnight to reach their maximum values around 10:00–11:00 LT in the dry seasons and two hours later in the rainy season (Fig. 6a). Thereafter, PM<sub>2.5</sub> decreases strongly until 15:00–16:00 LT, in the dry season and two hours later in the rainy season. Subsequently, PM<sub>2.5</sub> decreases very smoothly until reaching its minimum values around midnight. In addition, it is observed that in the cold dry season PM<sub>2.5</sub> concentrations are higher than in the other seasons. At JQRO the diurnal variations of PM<sub>2.5</sub> in the three seasons are very similar, they increase from early morning (02:00–03:00 LT) until reaching their maximum values around 08:00–09:00 LT in the dry seasons, and one hour later in the rainy season. The minimum values of PM<sub>2.5</sub> are presented around noon. Thereafter,

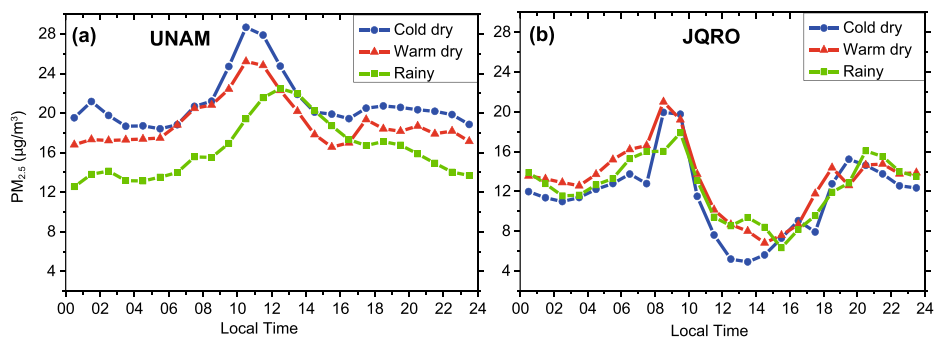


**Fig. 6** Diurnal cycles by season of the  $PM_{2.5}$  at (a) UNAM and (b) JQRO. The  $PM_{2.5}$  scale is the same in both observatories

they increase until reaching a second maxima between 19:00–21:00 LT, depending on the season (Fig. 6b).

### 3.3 Scattering coefficient ( $B_{scat}$ )

Table 3 shows the seasonal statistics of the scattering coefficient at UNAM and JQRO during all seasons. At UNAM, the average values of the scattering coefficient ( $B_{scat}$ ) were: 35.8, 27.1 and 31.3  $Mm^{-1}$ , while in JQRO were 10.9, 11.9 and 15.0  $Mm^{-1}$  during the cold dry, warm dry and rainy seasons, respectively. In JQRO, the rainy season presents the highest average scattering coefficient; unlike UNAM, where the cold dry season has the highest average. In JQRO, the averages of the scattering coefficient in the rainy season are approximately 38% and 26% higher than the averages in the warm dry and cold dry seasons; while in UNAM,  $B_{scat}$  in the cold dry season is around 14% higher than in the rainy season and 32% in the warm dry season.

Figure 7 (a–b) shows the seasonal diurnal variation of  $B_{scat}$  during the entire observation period, at UNAM and JQRO. At UNAM, the scattering coefficient increases rapidly from 05:00–06:00 LT until reaching its maximum values between 10:00–11:00 LT (dry seasons), and 12:00–13:00 LT (rainy season) (Fig. 7a). The increase of  $B_{scat}$  in the morning can be explained as a combination of vehicle emissions and photochemically generated secondary aerosols (Paredes-Miranda et al. 2009). For instance, photochemical formation of ammonium nitrate and secondary organic aerosol (SOA) contribute to the diurnal profile of the scattering coefficient (Marley et al. 2009). Also, scattering

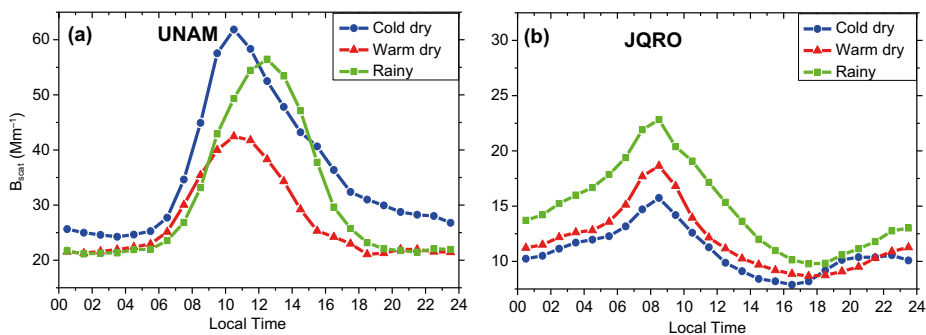


**Fig. 7** Diurnal cycles by season of  $B_{scat}$  at (a) UNAM and (b) JQRO. The  $B_{scat}$  scale at UNAM is twice that of JQRO



inorganic species with ammonium, sulfates, and nitrates could shape the diurnal pattern of aerosols (Salcedo et al. 2006).

In the same way, a rapid morning formation of SOA was observed due to photochemical processes in Mexico City (Salcedo et al. 2006; Volkamer et al. 2007; Hennigan et al. 2008a). Hennigan et al. (2008a) found that water-soluble organic carbon (WSOC) (or SOA) and nitrate were strongly correlated between 08:00 and 12:45 LT, and that SOA and nitrate concentration increases were caused by secondary production (~75–85%) and the entrainment of air in an expanding boundary layer (~15–25%). Similarly, Paredes-Miranda et al. (2009) estimated that until noon, about 75% of the aerosol mass and scattering is due to the photochemical production of secondary aerosol.

The subsequent fall of  $B_{\text{scat}}$  between 10:00 and 12:00 LT is related to the decrease in the concentration of particulate nitrate and SOA (Salcedo et al. 2006; Volkamer et al. 2007; Hennigan et al. 2008a). Approximately 65% of the decrease in nitrate and SOA concentrations occurs by dilution due to the expansion of the boundary layer and around 35% by the evaporation of the particles (Hennigan et al. 2008a). In general, the diurnal cycles of the  $B_{\text{scat}}$  are consistent with those of previous studies in Mexico City (Paredes-Miranda et al. 2009; Marley et al. 2009; Retama et al. 2015).

As shown in Fig. 7a, the values of  $B_{\text{scat}}$  during the cold dry season are higher than those of the warm dry and rainy seasons, except between 12:00 and 15:00 LT. The broader period of  $B_{\text{scat}}$  increase is probably due to the high amounts of water vapor during the rainy season (relative humidity 21% and 34% higher than in the warm dry and cold dry seasons, respectively) which allows the hygroscopic components of the aerosol, such as nitrates and sulfates (highly scattering) to take up more water vapor than in dry seasons, causing an increase in light scattering (Finlayson-Pitts and Pitts 2000; Nessler et al. 2005; Seinfeld and Pandis 2006).

Figure 7b shows the daily trends of the scattering coefficient at JQRO. During the three seasons, the  $B_{\text{scat}}$  follow similar diurnal trends, reaching their maximum values simultaneously at 08:00–09:00 LT. Thereafter, the  $B_{\text{scat}}$  decreases until reaching its minimum values in the afternoon hours, during the cold dry season at 16:00–17:00 LT, and at 17:00–18:00 LT in warm dry and rainy seasons.

The increase of  $B_{\text{scat}}$  up to its maxima can be attributed to the gradual increase of primary emissions of scattering aerosols and perhaps to the secondary aerosol carryover of the previous day. The cause of the subsequent decrease of  $B_{\text{scat}}$  could be due to the dilution (generated by the rapid development of the mixed-layer height), and ventilation. At JQRO the solar radiation increases more rapidly than at UNAM (Fig. 3c, d). A high solar radiation implies a faster development of the planetary boundary layer, which generates a strong dilution of particles. Another meteorological parameter that is important to analyze is wind speed. There is greater ventilation at JQRO than at UNAM. The hourly averages of wind speed generally double those observed in UNAM (Fig. 3e, f). The beginning of  $B_{\text{scat}}$  decrease coincides with the increase in wind speed, which suggests that the strong advection also contributes to the  $B_{\text{scat}}$  decrease. In addition to the relative low emissions in JQRO respect to Mexico City, dilution and ventilation favor the rapid fall of the concentration of gases and particles.

Several experiments have quantified the growth of particles with RH, called hygroscopic growth factor,  $g(\text{RH})$ ; or the resulting changes in the scattering coefficient, called scattering enhancement factor,  $f(\text{RH})$  (Howell et al. 2006). The scattering enhancement quantifies the magnitude of the change in  $B_{\text{scat}}$  due to water uptake and depends on the size and the chemical composition of the aerosol. The  $f(\text{RH})$  is defined as the ratio between the  $B_{\text{scat}}$  at a certain environmental RH and  $B_{\text{scat}}$  in dry conditions (Finlayson-Pitts and Pitts 2000; Titos et al. 2014).

Unfortunately, we do not have measurements of the particle size distribution to find hygroscopic growth; however, the simultaneous measurements of  $B_{\text{scat}}$  and RH allow estimating the effect of relative humidity on aerosol light scattering. To estimate  $f$  (RH = 85%), we evaluated  $B_{\text{scat}}$  measurements at different RH, but mainly <30% (minimizing the effect that the aerosol can absorb water at low RH and maintaining a reasonable number of observations), and between 80 and 90% RH (greater than the deliquescence relative humidity of the aerosol components). Table 4 shows the values of  $B_{\text{scat}}$  at HR < 30% and RH = 85%, and the factor  $f$  (RH = 85%) at UNAM and JQRO. During the cold dry season, the highest values of scattering enhancement factor are obtained, these values were 1.8 and 1.4 for UNAM and JQRO, respectively. This result suggests that at both sites, very hygroscopic small particles predominate (for example, ammonium nitrate and ammonium sulfate) which, when hydrated, grow to reach sizes where they are very efficient at light scattering.

At UNAM the lowest value of scattering enhancement factor was 0.8 and is obtained during the rainy season. This could be because a fraction of aerosols has a size distribution that would already be within the efficient range of light scattering, so that when hydrated it acquires a larger mass and a significant fraction of aerosols leave the scattering efficiency range. At JQRO the lowest value was 1.0 and is obtained in warm dry season. In general, the light scattering efficiency of individual particles is a non-linear function of particle size, with peaks of efficiency occurring between  $\sim 0.4$ – $1.4 \mu\text{m}$  particle diameter (Hegg et al. 1993). As particles grow when they hydrate, they can enter or leave the efficiency range depending on their initial dry size. Consequently, the factor that most influences hygroscopic growth is the position of the dry aerosol size distribution relative to the efficient light scattering particles size range.

**Influence of wind speed on the scattering coefficient** To analyze the influence of wind speed on the optical properties of particles, polar contour graphs are used. These are surface plots drawn in two dimensions of the form  $r(x)$ ,  $\theta(y)$  (polar coordinates) and associated with a third variable  $z$ , where the ranges of  $z$  values are distinguished by different colors. In the present study, the radial variable represents the wind speed (0–10 m/s), the angular variable the wind direction ( $0^\circ$ – $360^\circ$ ) and the color on the plot represents the magnitude of the optical property (scattering coefficient or absorption coefficient). The  $0^\circ$  direction means that the wind comes from the north towards the south;  $90^\circ$ ,  $180^\circ$  and  $270^\circ$  represent winds coming from the east, south and west, respectively. The black line around the center marks the relative frequency of wind direction. We define as “low speed” a wind speed between 0 and 2 m/s and a “high speed” when it is higher than 4 m/s. The first represents the transport of local emissions, while the second represents a regional transport (He et al. 2009; Han et al. 2009).

Figure 8(a–f) presents the wind dependence of the scattering coefficient for the three seasons at UNAM and JQRO. At UNAM a scale of values of the  $B_{\text{scat}}$  is defined using its

**Table 4** Scattering coefficient at RH = 85% and at dry conditions (RH < 30%), and scattering enhancement factor  $f$ (RH) at UNAM and JQRO

	UNAM			JQRO		
	Cold dry	Warm dry	Rainy	Cold dry	Warm dry	Rainy
$B_{\text{scat}}$ (RH = 85%) ( $\text{Mm}^{-1}$ )	50.1	35.0	21.6	10.6	10.6	17
$B_{\text{scat}}$ (RH < 30%) ( $\text{Mm}^{-1}$ )	28.1	24.3	28.6	7.4	10.3	13.4
$f$ (RH = 85%)	1.8	1.4	0.8	1.4	1.0	1.3

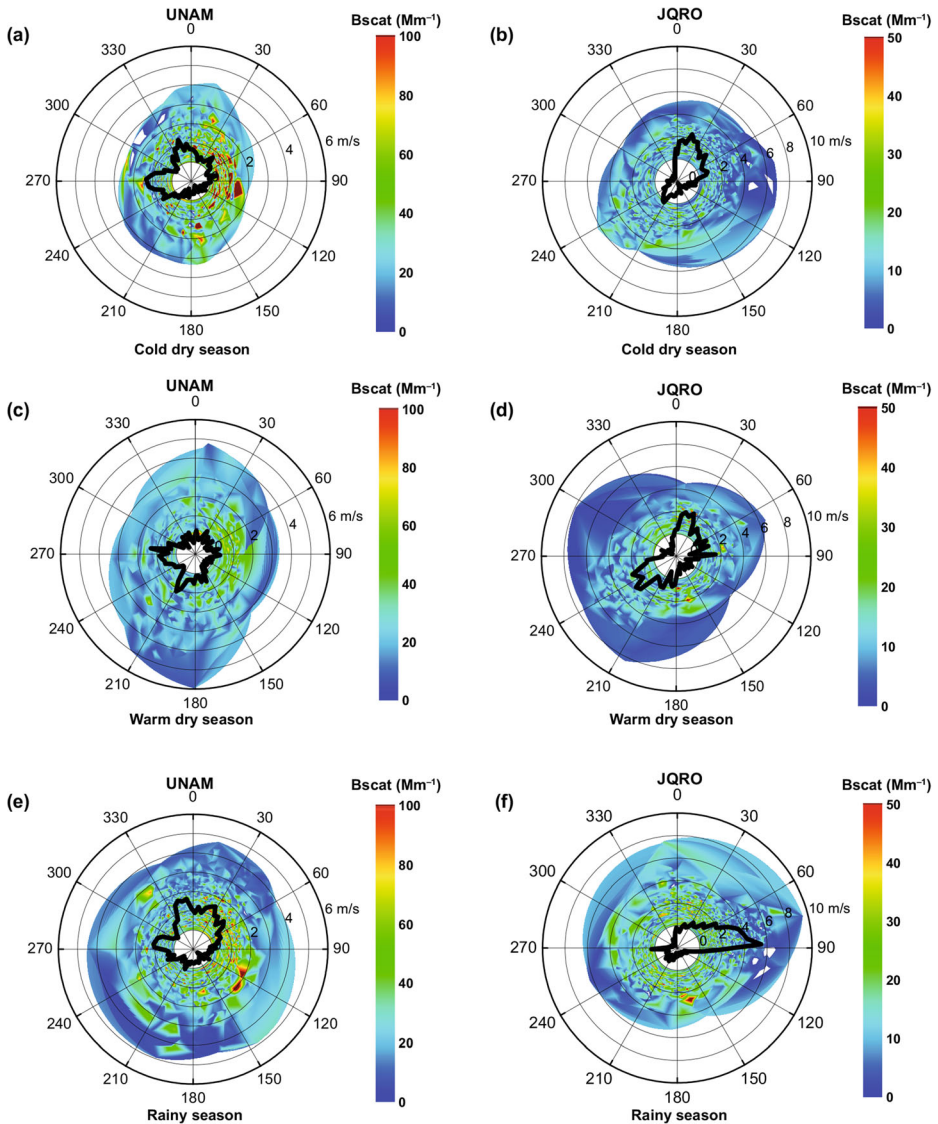
seasonal average value as a reference. Thus, a  $B_{\text{scat}}$  with values higher than  $100 \text{ Mm}^{-1}$  is a “ $B_{\text{scat}}$  *very high*”; with values between 50 and  $100 \text{ Mm}^{-1}$ , it is a “ $B_{\text{scat}}$  *high*”; of 20– $50 \text{ Mm}^{-1}$  as a “ $B_{\text{scat}}$  *intermediate*”, and for values lower than  $20 \text{ Mm}^{-1}$  as a “ $B_{\text{scat}}$  *low*”. The most frequent wind direction is from the west during the dry season (cold and warm), while during the rainy season, the winds prevail from the northeast. This result is consistent with previous studies (Jáuregui 1997, 2002). During the cold dry season (Fig. 8a), when the wind has a low speed and comes from the northeast or southeast, the values of  $B_{\text{scat}}$  *high* and *very high* predominate; while when they come from the southwest or northwest, the *low* and *intermediate* values of  $B_{\text{scat}}$  predominate. The warm dry season (Fig. 8c) presents *high*  $B_{\text{scat}}$  values when the winds are weak and come from the northeast or southeast, whereas when it comes from the opposite sector  $B_{\text{scat}}$  is *intermediate*. In the rainy season (Fig. 8e), when the wind speed is low and comes from the northeast the *high* and *very high*  $B_{\text{scat}}$  values predominate, while when it comes from the southwest or northwest, the  $B_{\text{scat}}$  values are *low* and *intermediate*. During the warm dry and rainy seasons, strong winds are present from the northeast and southeast with a *low*  $B_{\text{scat}}$ , suggesting that regional transport provides a mass of clean air to Mexico City. These results indicate that the important emissions of  $B_{\text{scat}}$  are local, with sources located between the northeast and southeast of the UNAM site.

To evaluate the influence of wind speed on the  $B_{\text{scat}}$  at JQRO, we used a  $B_{\text{scat}}$  scale of values equivalent to half the scale at UNAM. During dry seasons, the predominant direction of the wind is from the northeast (with a significant component of the southwest); while in the rainy season, the most frequent direction is from the east. During the cold dry season (Fig. 8b), when the wind is weak and comes from any direction, *high*  $B_{\text{scat}}$  values predominate. This result indicates that the emissions are local and the sources of the *high*  $B_{\text{scat}}$  values are located around the observation site. If the wind is strong and comes from the southwest, *high*  $B_{\text{scat}}$  values predominate, while when it comes from the northeast and southeast,  $B_{\text{scat}}$  is *low*. This indicates that regional transport from the southwest provides a mass of air that contains a large fraction of particles that scatter light. In the warm dry season (Fig. 8d), when the wind is weak and comes from the south or north,  $B_{\text{scat}}$  is *high*. If the wind comes from other directions,  $B_{\text{scat}}$  is *intermediate*. For strong winds, generally  $B_{\text{scat}}$  is *low*; except for the *intermediate*  $B_{\text{scat}}$  values when it comes from the southwest. This indicates that regional transport provides a clean air mass (except from the southwest). In the rainy season (Fig. 8f), when wind speed is weak and comes from any direction, *high*  $B_{\text{scat}}$  values predominate. In addition, it can be observed that when the winds come from the south at intermediate speeds (2–4 m/s) the highest values of  $B_{\text{scat}}$  were presented. These results confirm that  $B_{\text{scat}}$  values in the rainy season are higher than the values of dry seasons and show that the important  $B_{\text{scat}}$  sources are in the north and south of JQRO site.

### 3.4 Absorption coefficient ( $B_{\text{abs}}$ )

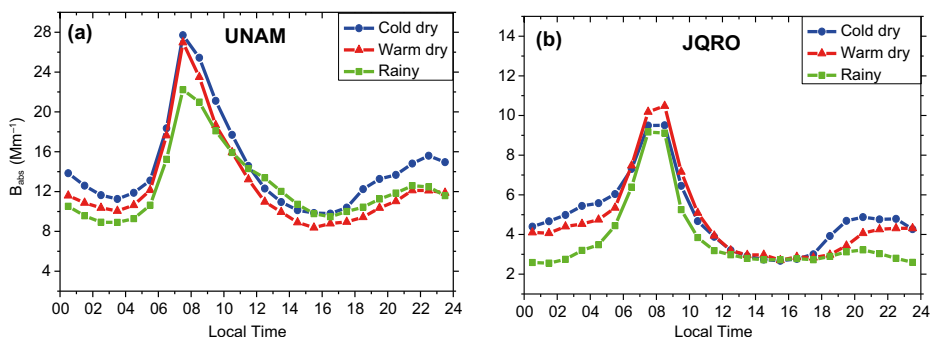
Table 3 shows the statistics of the absorption coefficient at UNAM and JQRO. In both sites, the seasonal average value of  $B_{\text{abs}}$  during the cold dry season is higher than the values of the other seasons, and the seasonal value of  $B_{\text{abs}}$  in the rainy season is the lowest. The seasonal averages of  $B_{\text{abs}}$  in UNAM are three times higher than JQRO during all seasons.

Figure 9(a–b) shows the daily seasonal variations of  $B_{\text{abs}}$  during the entire measurement period at UNAM and JQRO. At UNAM,  $B_{\text{abs}}$  diurnal trends are similar in all seasons, with two maxima (the first in the early morning and the second in the evening hours), and with two



**Fig. 8** Wind dependence of scattering coefficient, at Mexico City-UNAM (panels **a**, **c**, **e**), and Queretaro-JQRO (panels **b**, **d**, **f**)

minima (one in the afternoon and the other in early morning) (Fig. 9a). In the three seasons, a rapid increase of  $B_{abs}$  starts from 03:00–04:00 LT until reaching its maximum values at 07:00–08:00 LT. Thereafter,  $B_{abs}$  decreases to its minimum in the afternoon around 16:00–17:00 LT. A second daily maximum of  $B_{abs}$  appears at night, between 21:00–23:00 LT. Figure 9b shows the daily trends of the absorption coefficient at JQRO in all seasons. The  $B_{abs}$  diurnal cycles are similar, they begin with a gradual growth from midnight until reaching their maxima simultaneously at 08:00–09:00 LT (coinciding with the  $B_{scat}$  maxima). Thereafter,  $B_{abs}$  decreases very rapidly until 13:00–14:00 LT, maintaining minimum values until 17:00–18:00 LT. A second daily maximum of  $B_{abs}$  appears at evening, between 21:00–23:00 LT.



**Fig. 9** Daily cycles by season of Babs at (a) UNAM and (b) JQRO. The Babs scale at UNAM is twice that of JQRO

The discussion of black carbon (BC) is very similar to that of  $B_{\text{abs}}$ , since BC is obtained from  $B_{\text{abs}}$  divided by a mass-specific absorption cross section (MAC) of  $4.74 \text{ m}^2 \text{ g}^{-1}$ .

The diurnal variations of  $B_{\text{abs}}$  in both sites can be explained by the combination of two factors: emissions and meteorological conditions. At UNAM, the morning increase of the  $B_{\text{abs}}$  would be due to the increase in vehicle emissions, especially emissions of heavy-duty diesel vehicles (HDDVs) that are the most important sources of absorbent particles. Measurements of the density of vehicular traffic on a weekday in Mexico City show a weak circulation of vehicles in the early morning hours and a maximum density around 07:00–08:00 LT (Linan-Abanto, unpublished results). In addition, during the morning increase of  $B_{\text{abs}}$ , the solar radiation is zero or weak, which does not allow a great development of the boundary layer. A low mixing layer combined with a weak wind speed favors a large accumulation of primary particles and, therefore, high values of  $B_{\text{abs}}$ . The fall of  $B_{\text{abs}}$  to its minima values in the afternoon, could be related to both the increase in solar radiation (development of the boundary layer) (Fig. 3c, d), and the increase in wind speed (Fig. 3e, f). The second increase of  $B_{\text{abs}}$  in the afternoon, coincides with the fall in the height of the mixture layer from its maximum ( $\sim 3 \text{ km}$ ) at 17:00 LT in Mexico City (García-Franco et al. 2018).

**Influence of wind speed on the absorption coefficient** Figure 10 (a–f) shows the wind dependence of absorption coefficient for the three seasons at both sites. At UNAM, a scale of values of  $B_{\text{abs}}$  is defined using its seasonal average values (similar scale to obtained for  $B_{\text{scat}}$ ). A  $B_{\text{abs}}$  with values higher than  $20 \text{ Mm}^{-1}$  is a “ $B_{\text{abs}}$  very high”, with values between 14 and  $20 \text{ Mm}^{-1}$  is “ $B_{\text{abs}}$  high”, of 6–14  $\text{Mm}^{-1}$  is a “ $B_{\text{abs}}$  intermediate”, and for values lower than  $6 \text{ Mm}^{-1}$  as a “ $B_{\text{abs}}$  low”. During the cold dry season (Fig. 10a), when the wind is weak and comes from the sector between  $0^\circ$  and  $330^\circ$ , high and very high  $B_{\text{abs}}$  values predominate; while when it comes from the northwest the values of  $B_{\text{abs}}$  are intermediate. When the winds are intermediate and come from the southwest and northeast, the values of  $B_{\text{abs}}$  are high and intermediate, respectively. In the warm dry season (Fig. 10c), when the wind is weak and comes from any direction, a high and very high  $B_{\text{abs}}$  predominates. When the wind speed is high and comes from the northeast or the southeast, the  $B_{\text{abs}}$  is low and intermediate. In the rainy season (Fig. 10e), when the wind is weak and comes from any direction, the values of high  $B_{\text{abs}}$  predominate; except when it comes from the south, where  $B_{\text{abs}}$  is very high. When the winds are intermediate and come from all directions  $B_{\text{abs}}$  is intermediate. In general, during the three seasons it is observed that the pollution in Mexico City is due to emissions from local sources located around the measurement site.

To evaluate the influence of wind speed on  $B_{\text{abs}}$  in Queretaro, we used a  $B_{\text{abs}}$  values scale equal to half the scale in Mexico City. In Queretaro during the cold dry season (Fig. 10b), when



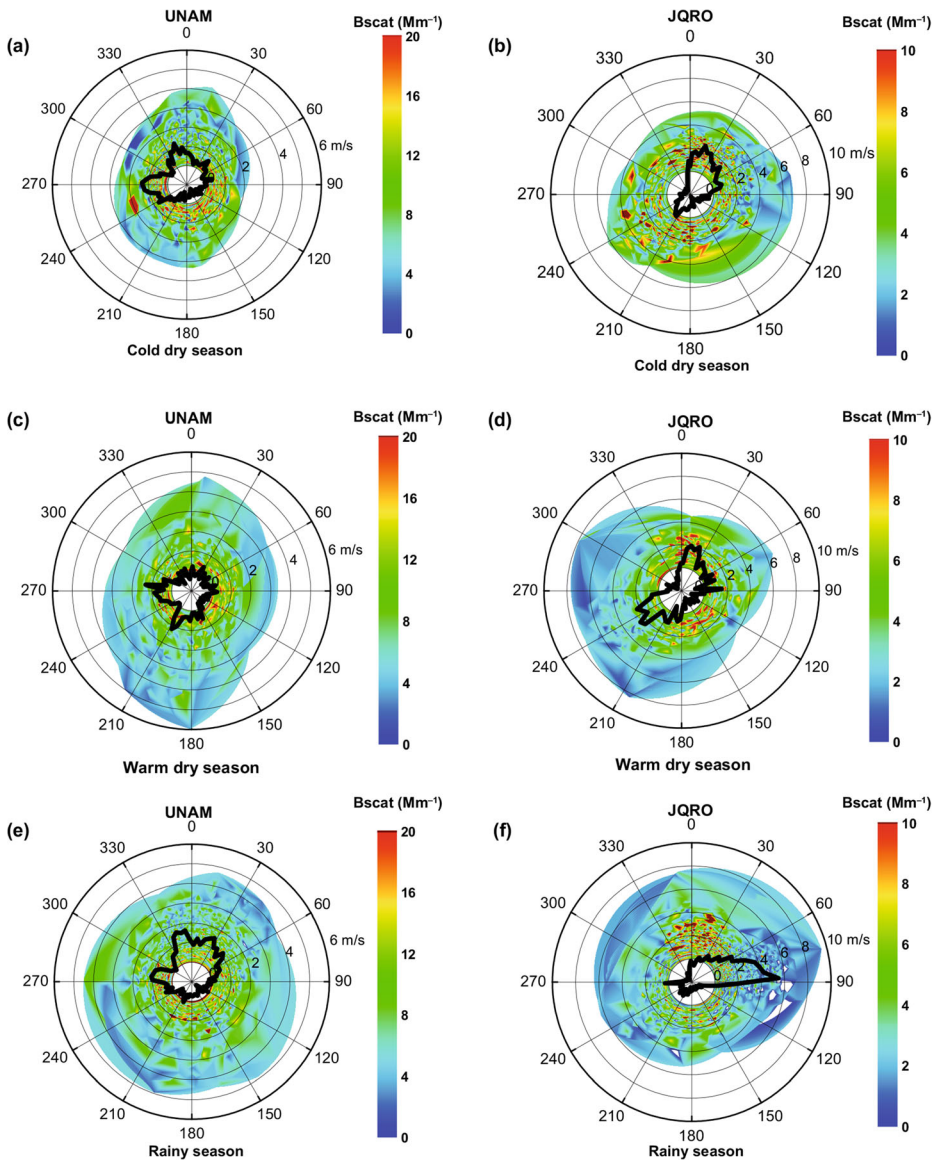


**Fig. 10** Wind dependence of absorption coefficient at Mexico City-UNAM (panels **a**, **c**, **e**), and Queretaro-JQRO (panels **b**, **d**, **f**)

the wind is weak and comes from the north or the south, *very high*  $B_{\text{abs}}$  predominate, in other directions,  $B_{\text{abs}}$  is *intermediate and high*. If the wind comes from southwest ( $240^{\circ}$ – $255^{\circ}$ ) with intermediate speed (2–4 m/s), the value of  $B_{\text{abs}}$  is *high and very high*. When the winds are strong and come from every direction, the  $B_{\text{abs}}$  that predominate are *intermediate*. In the warm dry season (Fig. 10d), when the wind is weak and comes from the north or the south,  $B_{\text{abs}}$  is *very high*. If the winds are strong or intermediate and come from the northeast  $B_{\text{abs}}$  is *intermediate*, while when it comes from the north,  $B_{\text{abs}}$  is *very high*. In the rainy season (Fig. 10f), when the winds are strong and come from any direction,  $B_{\text{abs}}$  is *intermediate*. *Very high*  $B_{\text{abs}}$  values are observed when the wind

comes from the north with weak and intermediate speed. These results indicate that there are significant emissions of absorbent aerosols from local sources located in the north and south of JQRO site.

### 3.5 Comparison of $B_{\text{scat}}$ and $B_{\text{abs}}$

At UNAM, when we compare the daily cycles of the scattering (Fig. 7a) and absorption (Fig. 9a) coefficients, it highlights the phase difference between their maxima. The scattering coefficient reaches its maximum 3 and 5 h after the maximum of absorption coefficient during the dry and rainy seasons, respectively. This result is consistent with previous optical properties studies in Mexico City Metropolitan Area, which reported the shifting between the maxima of the scattering and absorption coefficients (Salcedo et al. 2006; Marley et al. 2009; Paredes-Miranda et al. 2009). This gap arises from the difference of the formation processes of the absorbent and scattering aerosols. Absorbent particles, such as black carbon, are emitted directly into the atmosphere (primary emissions), while most scattering aerosols, such as sulfates and nitrates, are aerosols formed by gas-to-particle conversion processes and its formation requires more time (Paredes-Miranda et al. 2009; He et al. 2009; Lyamani et al. 2010).

At JQRO the maximum values of  $B_{\text{scat}}$  and  $B_{\text{abs}}$  are reached simultaneously. The time that  $B_{\text{scat}}$  takes to reach its maxima is considered as the time required for the formation of secondary particles in the atmosphere, while the maximum of the  $B_{\text{abs}}$  can be attributed to the primary particles (Paredes-Miranda et al. 2009). To explain what happens in Queretaro we analyze the formation of secondary aerosols and meteorological conditions. The formation of sulfate and nitrate and their contributions to  $\text{PM}_{2.5}$  mass depends on the emission mix of the precursors (i.e.,  $\text{SO}_2$ ,  $\text{NH}_3$ ,  $\text{NO}_x$ ), the levels of oxidants, the characteristics of preexisting aerosols/fog/cloud, and the meteorology (Pathak et al. 2009). Ammonia ( $\text{NH}_3$ ) is the main basic gas in the atmosphere and after  $\text{N}_2$  and  $\text{N}_2\text{O}$ , it is the most abundant nitrogen-containing compound in the atmosphere (Finlayson-Pitts and Pitts 2000; Seinfeld and Pandis 2006). When the ammonia reacts with nitric acid ( $\text{HNO}_3$ ), photochemical formation of ammonium nitrate occurs. For the photochemical production of nitric acid,  $\text{NO}_2$  and OH are required. In JQRO, concentrations of  $\text{NO}_2$  reach their maxima around 07:00–08:00 LT, two hours earlier than in UNAM (Fig. 4), when solar radiation is still weak. Subsequently, solar radiation increases but  $\text{NO}_2$  falls rapidly to minima values, which would not allow a significant photochemical production of nitric acid. Consequently, the formation of ammonium nitrate would not be significant, because for the formation of ammonium nitrate an important concentration of ammonia and nitric acid is required (Pathak et al. 2009). Although the photochemical production of  $\text{HNO}_3$  could be active after the maximum of  $\text{NO}_2$ , the photochemical production rate of ammonium nitrate would be insufficient to compensate for the loss of concentration due to dilution and advection.

At UNAM, the  $B_{\text{scat}}$  and  $B_{\text{abs}}$  show substantial morning increases by a factor of approximately 2.5 from the minimum to the maximum during all seasons. At JQRO, the  $B_{\text{scat}}$  is increased by a factor of approximately 1.6, while  $B_{\text{abs}}$  increases in the morning by a factor of 2.5 (dry seasons) and 3.5 (rainy season). This result indicates that local sources have a greater impact on the aerosol absorption coefficient than on its scattering coefficient. The maxima of  $B_{\text{abs}}$  at morning in all seasons can be explained by the large fraction of black carbon contained in aerosols of fresh combustion by diesel vehicles.

### 3.6 Single scattering albedo (SSA)

Single scattering albedo (SSA) is important because of its strong impact on direct aerosol radiative forcing. The direct effect of cooling or warming of the atmosphere by the scattering and absorbing particles depends on the SSA. Aerosols with an  $\text{SSA} > 0.95$  will result in a negative climate forcing and an overall cooling effect on the atmosphere, while an  $\text{SSA} < 0.86$  will have a positive climate forcing and an overall warming effect (Hansen et al. 1997; Marley et al. 2009). Highly scattering particles (nitrates and sulfates) have values of  $\text{SSA} \approx 1$ , while very absorbent aerosols (black carbon) exhibit values of around 0.3 (Arnott et al. 2000; Sheridan et al. 2005; Lewis et al. 2008). Table 3 shows the seasonal statistics of SSA at UNAM and JQRO. At UNAM, SSA seasonal average values in the three seasons are similar ( $\sim 0.66$ ). These results indicate that the seasonal values of SSA in both sites is below the critical value of 0.86 which determines the shift from cooling to warming, due to the significant presence of absorbing aerosols that promotes atmosphere warming. At JQRO, during the rainy season the highest SSA average of 0.78 is reached, which is 13% higher than the values of the dry season. This result suggests that Queretaro has a greater influence of the scattering particles than the absorbent ones during the rainy season compared to the dry seasons; probably due to a bigger hygroscopic growth due to the greater availability of water vapor in this season. During the three seasons, JQRO SSA values are higher than at UNAM.

The SSA is calculated from the measurements of scattering and extinction (scattering + absorption) of the light and is a function of aerosol chemical composition and morphology (Marley et al. 2009). In the present study the observations of SSA were made at only one wavelength (870 nm). Therefore, the daily cycle of SSA will be determined by the daily patterns of the scattering and absorption coefficients. Thus, the daily variations observed in the SSA during all seasons are due to the phase difference between the daily cycles of  $B_{\text{scat}}$  and  $B_{\text{abs}}$  (Lyamani et al. 2010). Figure 11 (a–b) shows the daily variations of SSA at UNAM and JQRO, during all seasons. At UNAM, the daily patterns of SSA are similar, with two maxima, one at early morning and the other in the afternoon; and two minima, the first in the morning and the second in the evening hours (Fig. 11a). During all seasons, the SSA decreases rapidly from first maxima obtained at 03:00–04:00 LT until its minima in the morning at 07:00–08:00 LT. Thereafter, the SSA increases until reaching maxima in the afternoon around 12:00–14:00 LT, depending on the season. The SSA decreases smoothly until reaching a second minimum at 22:00–23:00 LT during the dry seasons, and one hour earlier in the rainy season.

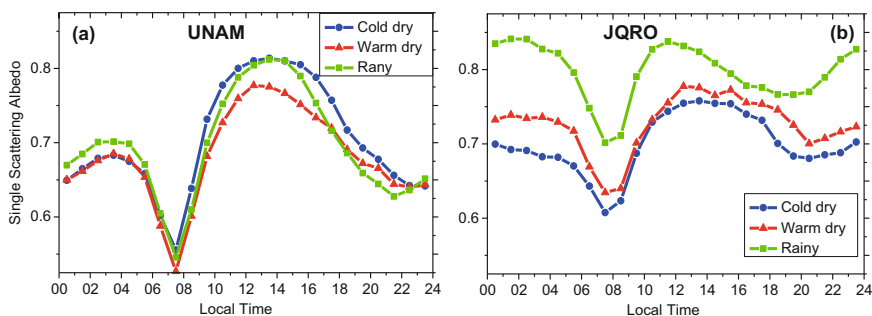


**Fig. 11** Diurnal cycles by season of the Single Scattering Albedo (SSA) in (a) UNAM and (b) JQRO. The SSA scale is the same in both observatories



Figure 11b shows the seasonal diurnal cycles of SSA at JQRO. The SSA decreases from a first maximum obtained in the early morning hours, until reaching its minimum values in the morning at 07:00–08:00 LT. Thereafter, the SSA increases until reaching maximum values at 11:00–12:00 LT during the rainy season, and between 12:00–14:00 LT in the dry seasons. Next, the SSA decreases slowly until it reaches its second minima around 20:00–21:00 LT during the dry seasons, and one hour before in the rainy season. These seasonal SSA trends are concordant with the seasonal trends of  $B_{\text{scat}}$  (Fig. 7b).

In general, the daily trends of SSA in both sites show two minima and two maxima. The first decrease in SSA early in the morning coincides with the first increase in  $B_{\text{abs}}$ , which reveals a greater relative importance of the light-absorbing particles (particles with BC) compared with the scattering particles. This probably is due to the greater fraction of heavy-duty diesel vehicles (HDDVs) to all types of vehicles (TVs) during early morning. Consequently, the SSA is more influenced by the changes of  $B_{\text{abs}}$  than of  $B_{\text{scat}}$ , early in the morning. This assertion is strengthened by the coincidence of the minima (and maxima) of SSA with the maxima (and minima) of  $B_{\text{abs}}$ , during all seasons. The second increase of the SSA to its maximum values in the afternoon indicates a greater relative contribution of light scattering aerosols, due to the continuous formation of photochemically generated secondary aerosols, and the relative decrease in the concentration of absorbing particles. In the three seasons, it is observed that the maxima SSA values are almost equal for several hours, when the dilution of the boundary layer is balanced by the formation of secondary aerosols, and continuous primary emissions of scattering and absorbent aerosols (Paredes-Miranda et al. 2009).

### 3.7 Correlations $B_{\text{scat}}$ vs. $\text{PM}_{2.5}$ , and mass-specific scattering cross section (MSC)

The scattering coefficient and  $\text{PM}_{2.5}$  are proportional to the concentration and size of the aerosol, so a strong correlation between these parameters is expected. Figure 12 (a–d) shows the scatterplots  $B_{\text{scat}}\text{--PM}_{2.5}$  during all the seasons and the entire observation period at UNAM. The slopes of the straight lines in these scatterplots are obtained by a linear fit with the least-squares method. The slope is an estimate of the mass-specific scattering cross section (MSC) and measures the change on  $B_{\text{scat}}$  when  $\text{PM}_{2.5}$  changes one unit. MSC derived by this method represent average conditions of an aerosol that could be changing because of variations in relative humidity, size distribution, and composition during the sampling period (Hand and Malm 2007). At UNAM the  $B_{\text{scat}}$  has a determination coefficient of 0.51 and slope of 1.76. The values of the slopes were 1.86, 1.35, and 1.88, during the cold dry, warm dry and rainy seasons, respectively. The MSC in the rainy season is slightly higher than in the cold dry season, and 39% higher than in the warm dry season.

Figure 13 (a–d) shows the scatterplots  $B_{\text{scat}}\text{--PM}_{2.5}$  in JQRO, during the three seasons and the entire observation period. The full period slope of the linear fit was 0.75 and a determination coefficient ( $R^2$ ) of 0.41. The values of the slopes were 0.57, 0.77 and 0.91, in the cold dry, warm dry and rainy seasons, respectively. The highest value of MSC is obtained in the rainy season and the lowest during the cold and dry season.

MSC values tend to be higher during polluted periods because of the greater influence of more efficient light scattering fine mode particles, and lower in clean conditions. (Hand and Malm 2007). Most of the light scattering by particles in the atmosphere is due to particles in the size range 0.1–1  $\mu\text{m}$  (Finlayson-Pitts and Pitts 2000). Several studies have shown that the fine particle mass and  $B_{\text{scat}}$  are related. Groblicki et al. (1981) finds a good correlation between  $B_{\text{scat}}$  and the fine particle mass, but not between  $B_{\text{scat}}$  and the coarse particle mass. Fine mode

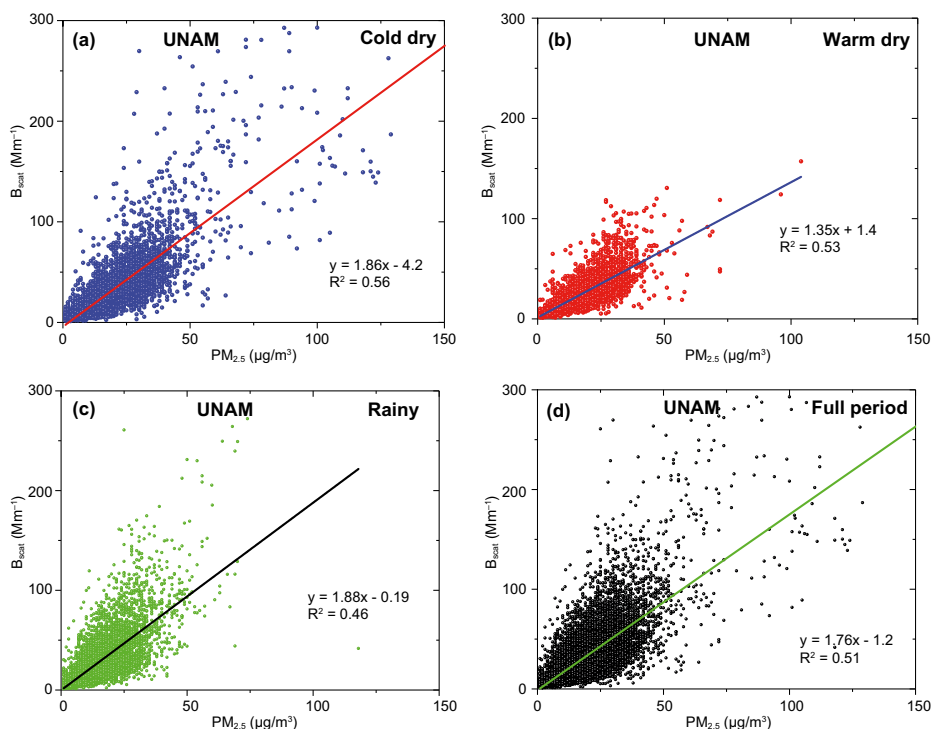


**Fig. 12** Correlations of Bscat-PM<sub>2.5</sub> during the three seasons and full period of measurement at Mexico City-UNAM

particles have higher MSC compared to coarse mode particles because smaller particles scatter light more efficiently (Hand and Malm 2007). The MSC values in UNAM are close to 2 m<sup>2</sup>/g, while in JQRO the MSC values are less than 1 m<sup>2</sup>/g. The largest MSC at UNAM than at JQRO indicates a difference in the composition of the aerosols. Mexico City, as a megacity, has more emissions and a much stronger (and longer) secondary aerosol formation rate than JQRO. Likewise, this result suggests that in Mexico City a greater fraction of the particles presents size distributions within the range of light scattering efficiency, while at JQRO the largest fraction of the particles is outside this range.

### 3.7.1 Diurnal variation of MSC

Figure 14 (a-b) shows the seasonal diurnal variation of the MSC during all seasons in both sites, obtained from the measurements of B<sub>scat</sub> and PM<sub>2.5</sub>. At UNAM the daily patterns of the MSC for the three seasons are similar (Fig. 14a). It increases very slowly from the early morning (01:00–02:00 LT) until 06:00–07:00 LT, probably related to the first daily emissions of fine particles in the city. Thereafter, the rise is faster until reaching its maximum at 09:00–10:00 LT, this rapid increase would be related to a greater predominance of fine particles. The high MSC values remain almost constant for several hours until 13:00–14:00 LT, this would be due to the high photochemical production rate of ammonium nitrate and SOA. At JQRO (Fig. 14b), diurnal cycles are less apparent than at UNAM. The maximum values of the MSC occur at midday, while the lowest values at the end of the afternoon.

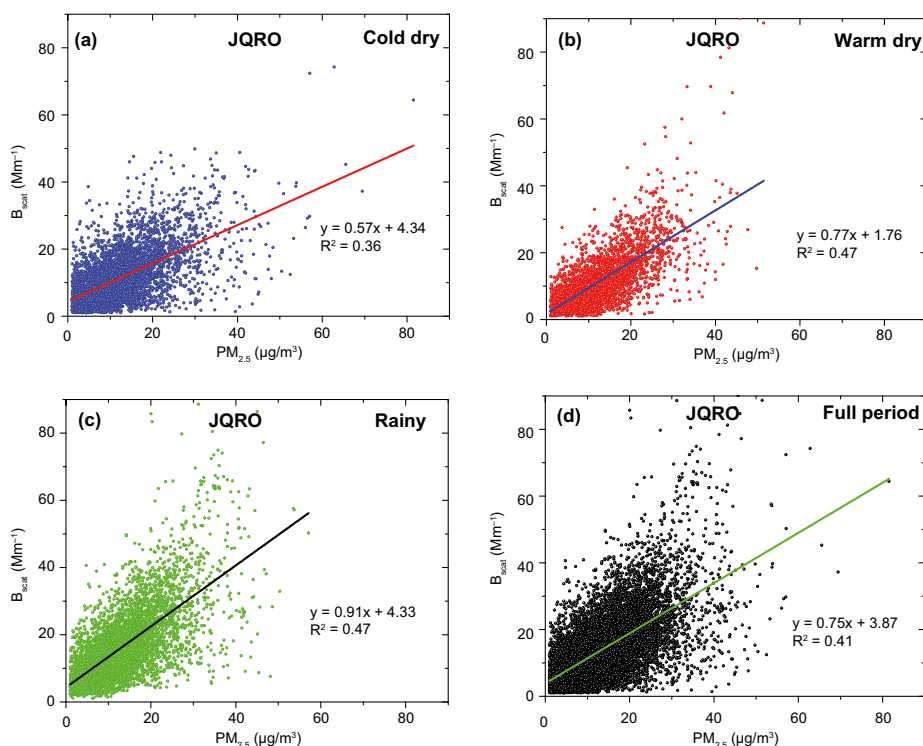


**Fig. 13** Correlations of  $B_{scat}$ - $PM_{2.5}$  during the three seasons and full period of measurement at Queretaro-JQRO

## 4 Conclusions

In this study, the measurements of optical properties, criteria pollutants ( $PM_{2.5}$ ,  $O_3$ , and  $NO_x$ ) have been evaluated at UNAM and JQRO atmospheric observatories of the RUOA, located in Mexico City (urban area), and Juriquilla-Queretaro (peri-urban area), respectively. We explain the differences in the daily cycles seasonal of the optical properties and criteria pollutants, based on changes in emission sources and local meteorology.

The air masses at UNAM and JQRO sites, were evaluated using the scatterplots of  $O_3$ - $NO_x$  concentrations. The concentrations of  $O_3$  and  $NO_x$  measured at UNAM fell in the VOC-limited region, typical of urban areas (air masses containing fresh emissions); while at JQRO, fell between the  $NO_x$ -limited region and the transition region, suggesting that most of the ozone measured at this site may be associated with photochemically aged air masses. This result suggests that ozone production at JQRO would be linked to photochemistry and transport; while at UNAM ozone would be mainly photochemically formed.

At UNAM, the diurnal cycles of  $B_{scat}$  are similar during the three seasons, with the highest seasonal average in the cold dry season. At JQRO, the  $B_{scat}$  values follow similar diurnal trends during the three seasons, reaching their maxima simultaneously at 08:00–09:00 LT. The highest seasonal average of the  $B_{scat}$  occurs during the rainy season. The cold dry season has the highest scattering enhancement factor at both sites, this result suggests that very small hygroscopic particles predominate, that when hydrated grow until reaching size distributions within the range of scattering efficiency of the light.

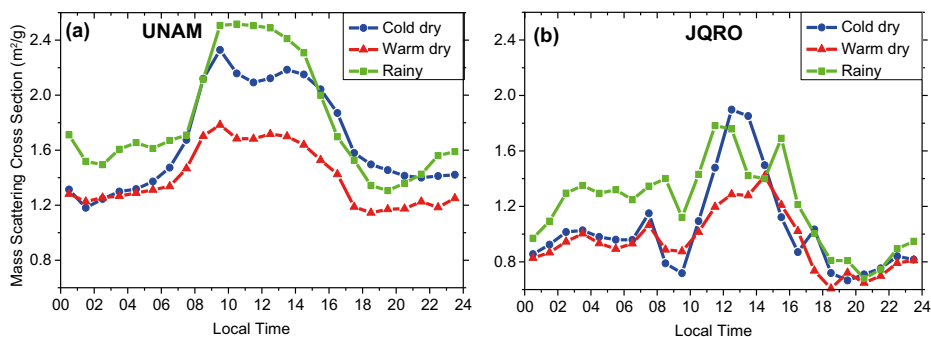


**Fig. 14** Diurnal variation by season of the Mass Scattering Cross Section (MSC) at (a) UNAM and (b) JQRO. The MSC scale is the same in both observatories

A clear diurnal cycle of the  $B_{\text{abs}}$  is observed at UNAM and JQRO during the three seasons, with two maxima and two minima, and the highest seasonal average during the cold dry season. The  $B_{\text{abs}}$  cycle is attributed to the diurnal evolution of the atmospheric boundary layer and local anthropogenic activities. The seasonal averages of  $B_{\text{abs}}$  at UNAM are greater by a factor of about 3 than those of JQRO.

At JQRO the maxima of  $B_{\text{abs}}$  and  $B_{\text{scat}}$  coincides; while at UNAM, the maximum values of  $B_{\text{scat}}$  have a delay of three hours during the dry seasons, and five hours in the rainy season. This phase difference arises due to the different formation processes of the aerosol. Absorbent aerosols are due to primary emissions, while most scattering aerosols are formed by gas-to-particle conversion processes and their formation requires more time.

$B_{\text{scat}}$  and  $B_{\text{abs}}$  show dependence on wind. At UNAM when the wind speed is weak, high values of  $B_{\text{scat}}$  and  $B_{\text{abs}}$  come from sources located in the northeast and southeast. High speeds are not important. This indicates that Mexico City is mainly influenced by local emission sources located northeast and southeast of the site.

At JQRO when the winds are weak and come from the north or the south, the highest values of  $B_{\text{scat}}$  and  $B_{\text{abs}}$  are observed. The intermediate and strong winds are frequent in Queretaro and generally provide air masses with low  $B_{\text{scat}}$  and  $B_{\text{abs}}$  values; however, when they come from the southwest  $B_{\text{scat}}$  and  $B_{\text{abs}}$  are high (cold dry season) and intermediate (warm and rainy seasons). This result suggests that Queretaro air would be influenced by local sources (located to the north and south) and by aerosols transported regionally.

The daily seasonal trends of the SSA at UNAM and JQRO follow similar diurnal trends during the three seasons, with two minima and two maxima. The decrease in SSA reveals a greater importance of the absorbing aerosols. The subsequent increase of the SSA indicates a greater contribution of the scattering aerosols. At JQRO, the rainy season presents the highest SSA average of 0.78 (13% higher than the values of the dry seasons). JQRO presents higher SSA values than UNAM ( $\sim 0.66$ ) during all season; but in both sites the SSA values are below the critical value of 0.86 which determines the shift from cooling to warming.

The MSC values in UNAM are close to  $2 \text{ m}^2/\text{g}$ , while in JQRO the MSC values are less than  $1 \text{ m}^2/\text{g}$ . The largest MSC at UNAM than at JQRO, suggests that in Mexico City a greater fraction of the particles presents size distributions within the range of light scattering efficiency, while at JQRO the largest fraction of the particles is outside this range.

In general, JQRO has a profoundly different behavior with respect to  $\text{NO}_x$  and VOC sensitivity, and the MSC is considerably lower than at UNAM. As a megacity, Mexico City has much more emissions and likely a higher proportion of emissions from HDDV leading to

high BC concentration and perhaps VOCs emissions. Mexico City has a much stronger secondary aerosol formation rate than Queretaro. Wind speeds in Mexico City are generally lower than in Queretaro, giving more time for secondary aerosol formation and larger pollution buildup. These results confirm the high levels of fine particles, the higher photochemical formation rate of ozone and the secondary aerosols that a megacity presents, such as Mexico City, are compared to a peri-urban site, such as JQRO.

**Acknowledgments** Rafael Liñán Abanto expresses his gratitude to Programa de Posgrado en Ciencias de la Tierra, UNAM and CONACyT for his Ph.D. scholarship. We acknowledge Isabel Saavedra who revised the English translation of the manuscript and technical assistance, and Bertha Mar for her help in preparing the maps. Authors, also want to thank Pietro Villalobos for his help editing the figures and images.

## References

- Arnott, W.P., Moosmüller, H., Rogers, C.F., Jin, T., Bruch, R.: Photoacoustic spectrometer for measuring light absorption by aerosols: instrument description. *Atmos. Environ.* **33**, 2845–2852 (1999)
- Arnott, W.P., Moosmüller, H., Walker, J.W.: Nitrogen dioxide and kerosene-flame soot calibration of photoacoustic instruments for measurement of light absorption by aerosols. *Rev. Sci. Instr.* **71**(7), 4545–4552 (2000)
- Bond, T.C., Bergstrom, R.W.: Light absorption by carbonaceous particles: an investigative review. *Aerosol Sci. Technol.* **40**, 27–67 (2006). <https://doi.org/10.1080/02786820500421521>
- Bond, T.C., Doherty, S.J., Fahey, D.W., Forster, P.M., Berntsen, T., DeAngelo, B.J., Flanner, M.G., Ghan, S., Kärcher, B., Koch, D., Kinne, S., Kondo, Y., Quinn, P.K., Sarofim, M.C., Schultz, M.G., Schultz, M., Venkataraman, C., Zhang, H., Zhang, S., Bellouin, N., Guttikunda, S.K., Hopke, P.K., Jacobson, M.Z., Kaiser, J.W., Klimont, Z., Lohmann, U., Schwarz, J.P., Shindell, D., Storelvmo, T., Warren, S.G., Zender, C.S.: Bounding the role of black carbon in the climate system: a scientific assessment. *Journal Geophysical Research:Atmospheres*. **118**, 5380–5552 (2013). <https://doi.org/10.1002/jgrd.50171>
- Borja-Aburto V.H., Castillejos, M., Gold, D.R., Bierzwinski, S., and Loomis, D., (1998). Mortality and ambient fine particles in Southwest Mexico City, 1993–1995. *Environ. Health Perspect.*, Vol 106, N° 12, 845–855, doi: <https://doi.org/10.1289/ehp.106-1533229>
- Bravo, J.L., Azpra, E., Zarzaluqui, V., Gay, C.: Some variations of the rainfall in Mexico City from 1954 to 1988 and their statistical significance. *Atmósfera*. **27**(4), 367–376 (2014). <https://doi.org/10.20937/ATM.2014.27.04.03>
- Burgos, R.G., Johnson, J.: Why Querétaro? The development of an aeronautical manufacturing cluster in Central Mexico. *Thunderbird International Business Review*. **60**(3), 251–263 (2016). <https://doi.org/10.1002/tic.21844>
- Castro, T., Ruiz-Suárez, L.G., Molina, J.M., Ruiz Suárez, J.C., Montero, M.: Sensitivity analysis of UV radiation transfer model and experimental photolysis rates of NO<sub>2</sub> in the atmosphere of Mexico City. *Atmos. Environ.* **30**(4), 609–620 (1997)
- Chameides, W. L., F. Fehsenfeld, S. Sillman and G. Hübler (1994). Evaluation of the Relative Contribution of VOCs and NO<sub>x</sub> to Ozone Formation in Rural and Urban Areas. Southern Oxidant Study; 1993 Data analysis report. F. Fehsenfeld, J. Meagher and E. Cowling. Raleigh, N.C., North Carolina State University: 92
- Corr, C.A., Krotkov, N., Madronich, S., Slusser, J.R., Holben, B., Gao, W., Flynn, J., Lefer, B., Kreidenweis, S.M.: Retrieval of aerosol single scattering albedo at ultraviolet wavelengths at the T1 site during MILAGRO. *Atmos. Chem. Phys.* **9**, 5813–5827 (2009). <https://doi.org/10.5194/acp-9-5813-2009>
- De Foy, B., Caetano, E., Magaña, V., Zitiácuaro, A., Cárdenas, B., Retama, A., Ramos, R., Molina, L.T., Molina, M.J.: Mexico City basin wind circulation during the MCMA-2003 field campaign. *Atmos. Chem. Phys.* **5**, 2267–2228 (2005). <https://doi.org/10.5194/acp-5-2267-2005>
- Dockery, D.W., Pope, C.A.: Epidemiology of acute health effects: summary of time-series. In: *Particles in our Air: Concentration and Health Effects*, Edited by: Wilson, R. and Spengler, J. D., Harvard University Press, Cambridge, MA, USA, 123–147 (1996)
- Dunlea, E.J., Hemdon, S.C., Nelson, D.D., Volkamer, R.M., San Martini, F., Sheehy, P.M., Zahniser, M.S., Shorter, J.H., Wormhoudt, J.C., Lamb, B.K., Allwine, E.J., Gaffney, J.S., Marley, N.A., Grutter, M., Marquez, C., Blanco, S., Cardenas, B., Retama, A., Villegas, C.R.R., Kolb, C.E., Molina, L.T., Molina, M.J.: Evaluation of nitrogen dioxide chemiluminescence monitors in a polluted urban environment. *Atmos. Chem. Phys.* **7**(10), 2691–2704 (2007). <https://doi.org/10.5194/acp-7-2691-2007>

- Finlayson-Pitts, B., Pitts, J.: Chemistry of the Upper and Lower Atmosphere: Theory, Experiments and Applications, First edn. Academic Press (2000)
- Flores, J., Michel, R., Bar-or, Z., Bluvshstein, N., Abo-Riziq, A., Kostinski, A., Bormann, S., Koren, I., Koren, I., Rudich, Y.: Absorbing aerosols at high relative humidity: linking hygroscopic growth to optical properties. *Atmos. Chem. Phys.* **12**, 5511–5521 (2012). <https://doi.org/10.5194/acp-12-5511-2012>
- Foster, P., Ramaswamy, V., Artaxo, P., Bernsten, T., Betts, R., Fahey, D. W., Haywood, J., Lean, J., Lowe, D. C., Myhre, G., Nganga, J., Prinn, R., Raga, G., Schulz, M., and Van Dorland, R.: Changes in Atmospheric Constituents and in Radiative Forcing, in: Climate Change 2007: The Physical Science Basis, Contribution of Working Group I to the Fourth Assessment Report of the Intergovernmental Panel on Climate Change, edited by: Solomon, S., Qin, D., Manning, M., Chen, Z., Marquis, M., Averyt, K. B., Tignor, M., and Miller, H. L., Cambridge University Press, Cambridge, United Kingdom and New York, NY, USA, 2007
- Fujita EM, Campbell DE, Stockwell W, Keislar RE, Zielinska B, Sagebiel JC, et al. Weekend/ weekday Ozone Observations in the South Coast Air Basin; Volume II — Analysis of Air Quality Data. Reno, NV: Desert Research Institute; 2002
- García-Franco, J.L., W. Stremme, A. Benzanilla, A. Ruiz-Angulo, M. Grutter: Variability of the Mixed-Layer Height Over Mexico City. *Boundary Layer Meteorology*, doi:<https://doi.org/10.1007/s10546-018-0334-x>, 2018.)
- García-Yee, J.S., Torres-Jardón, R., Barrera-Huertas, H., Castro, T., Peralta, O., García, M., Gutiérrez, W., Robles, M., Torres-Jaramillo, A., Ortíz, A., Ruiz-Suárez, L.G.: Characterization of NO<sub>x</sub>-ox relationships during daytime interchange of air masses over a mountain pass in the Mexico City megalopolis. *Atmospheric Environment*. **177**, 100–110 (2018). <https://doi.org/10.1016/j.atmosenv.2017.11.017>
- Groblicki, P.J., Wolff, G.T., Countess, R.J.: Visibility reducing species in the Denver Brown cloud. I. *Atmos. Environ.* **15**, 2473–2484 (1981)
- Han, S., Kondo, Y., Oshima, N., Takegawa, N., Miyazaki, Y., Hu, M., Lin, P., Deng, Z., Zhao, Y., Sugimoto, N., Wu, Y.: Temporal variations of elemental carbon in Beijing. *J. Geophys. Res.* **114**, D23202 (2009). <https://doi.org/10.1029/2009JD012027>
- Hand, J.L., Malm, W.C.: Review of aerosol mass scattering efficiencies from ground-based measurements since 1990. *J. Geophys. Res.* **112**, D16203 (2007). <https://doi.org/10.1029/2007JD008484>
- Hansen, J., Sato, M., Ruedy, R.: Radiative forcing and climate response. *J. Geophys. Res.* **102**(D6), 6831–6864 (1997). <https://doi.org/10.1029/96JD03436>
- Hansen, James Makiko Sato, Reto Ruedy, Andrew Lacis, and Valdar Oinas: Global warming in the twenty-first century: An alternative scenario PNAS August 29, 2000 vol. 97 No. 18 9875–988. Article published online before print: Proc. Natl. Acad. Sci. USA, <https://doi.org/10.1073/pnas.170278997>
- He, X., Li, C.C., Lau, A.K.H., Deng, Z.Z., Mao, J.T., Wang, M.H., Liu, X.Y.: An intensive study of aerosol optical properties in Beijing urban area. *Atmos. Chem. Phys.* **9**, 8903–8915 (2009). <https://doi.org/10.5194/acp-9-8903-2009> Res
- Hegg, D., Larson, T., Yuen, P.-F.: A theoretical study of the effect of relative humidity on light scattering by tropospheric aerosols. *J. Geophys. Res.* **98**, 18435–18439 (1993). <https://doi.org/10.1029/93JD01928>
- Heintzenberg, J., Charlson, R.J., Clarke, A.D., Liousse, C., Ramaswamy, V., Shine, K.P., Wendisch, M., Helas, G.: Measurements and modeling of aerosol single-scattering albedo: Progress, problems and prospects. *Beitr. Phys. Atmos.* **70**, 249–263 (1997)
- Hennigan, C.J., Sullivan, A.P., Fountoukis, C.I., Nenes, A., Hecobian, A., Vargas, O., Peltier, R.E., Case Hanks, A.T., Huey, L.G., Lefer, B.L., Russell, A.G., Weber, R.J.: On the volatility and production mechanisms of newly formed nitrate and water soluble organic aerosol in Mexico City. *Atmos. Chem. Phys.* **8**(14), 3761–3768 (2008a). <https://doi.org/10.5194/acp-8-3761-2008>
- Hennigan, C.J., Bergin, M.H., Dibb, J.E., Weber, R.J.: Enhanced secondary organic aerosol formation due to water uptake by fine particles. *Geophys. Res. Lett.* **35**, L18801 (2008b). <https://doi.org/10.1029/2008GL035046>
- Horvath, H.: Estimation of the average visibility in Central Europe. *Atmos. Environ.* **29**, 241–246 (1995). [https://doi.org/10.1016/1352-2310\(94\)00236-E](https://doi.org/10.1016/1352-2310(94)00236-E)
- Howell, S.G., Clarke, A.D., Shinozuka, Y., Kapustin, V., McNaughton, C.S., Huebert, B.J., Doherty, S.J., Anderson, T.L.: Influence of relative humidity upon pollution and dust during ACE-Asia: size distributions and implications for optical properties. *J. Geophys. Res.* **111**, D06205 (2006). <https://doi.org/10.1029/2004JD005759>
- INEGI (2018). Instituto Nacional de Estadística Geografía e Historia. Retrieved January 18, 2018, from <https://www.inegi.org.mx/default.aspx>
- IPCC (Intergovernmental Panel on Climate Change) (2013) Clouds and aerosols in: climate change 2013: the physical science basis. Contribution of working group I to the fifth assessment report of the intergovernmental panel on climate change. Cambridge University press, Cambridge; United Kingdom and New York, NY, USA
- Jáuregui, E.: The urban climate of Mexico City. *Erdkunde*. **28**(4), 298–307 (1973)
- Jáuregui, E.: Heat island development in Mexico City. *Atmos. Environ.* **31**, 3821–3831 (1997). [https://doi.org/10.1016/S1352-2310\(97\)00136-2](https://doi.org/10.1016/S1352-2310(97)00136-2)



- Jáuregui, E.: The climate of the Mexico City Air Basin: its effects on the formation and transport of pollutants. In: Fenn, M.E., de Bauer, L.I., Hernandez-Tejeda, T. (eds.) *Ecological Studies. Urban Air Pollution and Forest*, vol. 56, pp. 86–117. Chapter 5. Springer, New York (2002). [https://doi.org/10.1007/978-0-387-22520-3\\_5](https://doi.org/10.1007/978-0-387-22520-3_5)
- Kaufman, Y.J., Koren, I., Remer, L.A., Rosenfeld, D., Rudich, Y.: The effect of smoke, dust, and pollution aerosol on shallow cloud development over the Atlantic Ocean. *Proc. Natl. Acad. Sci. U. S. A.* **102**(32), 11207–11212 (2005). <https://doi.org/10.1073/pnas.0505191102>
- Marley, M. S. 2000, in ASP Conf. Ser. 212, *From Giant Planets to Cool Stars*, ed. C. A. Griffith & M. S. Marley (San Francisco: ASP), 152
- Marley, N.A., Gaffney, J.S., Castro, T., Salcido, A., Frederick, J.: Measurements of aerosol absorption and scattering in the Mexico City metropolitan during the MILAGRO field campaign: a comparison of results from the T0 and T1 sites. *Atmos. Chem. Phys.* **9**, 189–206 (2009). <https://doi.org/10.5194/acp-9-189-2009>
- Nessler, Remo. Ernest Weingartner., Urs Baltensperger.: Effect of humidity on aerosol light absorption and its implications for extinction and the single scattering albedo illustrated for a site in the lower free troposphere. *Journal of Aerosol Science* Volume 36, Issue 8, August 2005, Pages 958–972 <https://doi.org/10.1016/j.jaerosci.2004.11.012>
- Lewis, K., Arnott, W.P., Moosmüller, H., Wold, C.E.: Strong spectral variation of biomass smoke light absorption and single scattering albedo observed with a novel dual wavelength photoacoustic instrument. *J. Geophys. Res.* **113**, D16203 (2008). <https://doi.org/10.1029/2007JD009699>
- Liu, S.C., McKeen, S.A., Madronich, S.: Effect of anthropogenic aerosols on biologically active ultraviolet radiation, *geophysical research letters* Volume18, Issue12 December. **1991**, 2265–2268 (1991). <https://doi.org/10.1029/91GL02773>
- Lyamani, H., Olmo, F.J., Alados-Arboledas, L.: Physical and optical properties of aerosols over an urban location in Spain: seasonal and diurnal variability. *Atmos. Chem. Phys.* **10**, 239–254 (2010). <https://doi.org/10.5194/acp-10-239-2010>
- Paredes-Miranda, G., Arnott, W.P., Jimenez, J.L., Aiken, A.C., Gaffney, J.S., Marley, N.A.: Primary and secondary contributions to aerosol light scattering and absorption in Mexico City during the MILAGRO 2006 campaign. *Atmos. Chem. Phys.* **9**, 3721–3730 (2009). <https://doi.org/10.5194/acp-9-3721-2009>
- Pathak, R.K., Wu, W.S., Wang, T.: Summertime PM<sub>2.5</sub> ionic species in four major cities of China: nitrate formation in an ammonia-deficient atmosphere. *Atmos. Chem. Phys.* **9**, 1711–1722 (2009). <https://doi.org/10.5194/acp-9-1711-2009>
- Peralta, O., Baumgardner, D. and Raga, G.: Spectrothermography of carbonaceous particles, *J. Atmos. Chem.*, published on line, <https://doi.org/10.1007/s10874-007-9070-1>, 2007, 57, 153, 169
- Pope III, C.A., Dockery, D.W.: Health effects of fine particulate air pollution: lines that connect. *J. Air Waste Manage. Assoc.* **56**, 709–742 (2006). <https://doi.org/10.1080/10473289.2006.10464485>
- Retama, A., Baumgardner, D., Raga, G.B., McMeeking, G.R., Walker, J.W.: Seasonal and diurnal trends in black carbon properties and co-pollutants in Mexico City. *Atmos. Chem. Phys.* **15**, 9693–9709 (2015). <https://doi.org/10.5194/acp-15-9693-2015>
- Ruiz Suárez, L., Longoria, R., Hernandez, F., Segura, E., Trujillo, A., Conde, C.: Emisiones biogénicas de Hidrocarburos No-metano y de Oxido Nítrico en la Cuenca del Valle de México. *Atmosfera.* **12**, 89–100 (1999). <https://doi.org/10.3390/atmos9060223>
- Salcedo, D., Onasch, T.B., Dzepina, K., Canagaratna, M.R., Zhang, Q., Huffman, J.A., DeCarlo, P.F., Jayne, J.T., Mor-timer, P., Worsnop, D.R., Kolb, C.E., Johnson, K.S., Zuberi, B., Marr, L.C., Volkamer, R., Molina, L.T., Molina, M.J., Cardenas, B., Bernabe, R.M., Marquez, C., Gaffney, J.S., Marley, N.A., Laskin, A., Shutthanandan, V., Xie, Y., Brune, W., Leshner, R., Shirley, T., Jimenez, J.L.: Characterization of ambient aerosols in Mexico City during the MCMA-2003 campaign with aerosol mass spectrometry: results from the CENICA super-site. *Atmos. Chem. Phys.* **6**, 925–946 (2006). <https://doi.org/10.5194/acp-6-925-2006>
- Salcedo, D., Castro, T., Ruiz-Suárez, L.G., García-Reynoso, A., Torres-Jardón, R., Torres-Jaramillo, A., Mar-Morales, B.E., Salcido, A., Celada, A.T., Carreón-Sierra, S., Martínez, A.P., Fentanes-Arriaga, O.A., Deustúa, E., Ramos-Villegas, R., Retama-Hernández, A., Saavedra, M.I., Suárez-Lastra, M.: Study of the regional air quality south of Mexico City (Morelos state). *Sci. Total Environ.* **414**, 417–432 (2012). <https://doi.org/10.1016/j.scitotenv.2011.09.041>
- Seinfeld, J., Pandis, S.: *Atmospheric Chemistry and Physics: from Air Pollution to Climate Change*, Second edn. John Wiley & Sons, Inc (2006)
- Schwartz, S. E., Arnold, F., Blanchet, J. P., Durke, P. A., Hofmann, D. J., Hoppel, W. A., King, M. D., Lacis, A. A., Nakajima, T., Ogren, J. A., Toon, O. B., and Wendisch, M.: Group report: connections between aerosol properties and forcing of climate, in: *Aerosol of Climate*, edited by: Heintzenberg, J. and Charlson, R. J., Wiley, New York, 251–280, 1995
- Sheridan, P.J., Arnott, W.P., Ogren, J.A., Anderson, B.E., Atkinson, D.B., Covert, D.S., Moosmüller, H., Petzold, A., Schmid, B., Strawa, A.W., Varma, R., Virkkula, A.: The Reno aerosol optics study: an evaluation of

- aerosol absorption measurement methods. *Aerosol Sci. Technol.* **39**, 1–16 (2005). <https://doi.org/10.1080/027868290901891>
- Sillman, S., He, D.: Some theoretical results concerning O<sub>3</sub>-NO<sub>x</sub>-VOC chemistry and NO<sub>x</sub>-VOC indicators. *Journal of Geophysical Research: Atmospheres*. **107**(D22), (2002). <https://doi.org/10.1029/2001JD001123>
- Titos, G., Lyamani, H., Cazorla, A., Sorribas, M., Foyo-Moreno, I., Wiedensohler, A., Alados-Arboledas, L.: Study of the relative humidity dependence of aerosol light-scattering in southern Spain. *Tellus B: Chemical and Physical Meteorology*. **66**(1), 24536 (2014). <https://doi.org/10.3402/tellusb.v66.24536>
- Torres-Jardón, R., García-Reynoso, J.A., Jazcilevich, A., Ruiz-Suárez, L.G., Keener, T.C.: Assessment of the ozone–nitrogen oxide–volatile organic compound sensitivity of Mexico City through an indicators-based approach: measurements and numerical simulations comparison. *J Air Waste Manag Assoc.* **59**, 1155–1172 (2009)
- Volkamer, R., San Martini, F., Molina, L.T., Salcedo, D., Jimenez, J.L., Molina, M.J.: A missing sink for gas-phase glyoxal in Mexico City: formation of secondary organic aerosol. *Geophys. Res. Lett.* **34**, L19807 (2007). <https://doi.org/10.1029/2007GL030752>
- Williams, J., de Reus, M., Krejci, R., Fischer, H., Ström, J.: Application of the variability-size relationship to atmospheric aerosol studies: estimating aerosol lifetimes and ages. *Atmos. Chem. Phys.* **2**, 133–145 (2002). <https://doi.org/10.5194/acp-2-133-2002>
- Zaveri, Rahul A., Berkowitz, Carl M., Kleinman, Lawrence I., Springston, Stephen R., Doskey, Paul V., Lonneman, William A. and Spicer, Chester W: Ozone production efficiency and NO<sub>x</sub> depletion in an urban plume: Interpretation of field observations and implications for evaluating O<sub>3</sub>-NO<sub>x</sub>-VOC sensitivity. *Journal of Geophysical Research*, Vol. 108, NO. D14, 4436, 2003. doi:<https://doi.org/10.1029/2002JD003144>

**Publisher's note** Springer Nature remains neutral with regard to jurisdictional claims in published maps and institutional affiliations.

## Affiliations

Rafael N. Liñán-Abanto<sup>1,2,3</sup> · O. Peralta<sup>1</sup> · D. Salcedo<sup>4</sup> · L. G. Ruiz-Suárez<sup>1</sup> · P. Arnott<sup>5</sup> · G. Paredes-Miranda<sup>5</sup> · H. Alvarez-Ospina<sup>1,6</sup> · T. Castro<sup>1</sup>

<sup>1</sup> Centro de Ciencias de la Atmósfera, Universidad Nacional Autónoma de México, Ciudad de México, Mexico

<sup>2</sup> Departamento de Física, Facultad de Ciencias, Universidad Nacional Jorge Basadre G, Tacna, Peru

<sup>3</sup> Programa de Posgrado en Ciencias de la Tierra, Universidad Nacional Autónoma de México, Ciudad de México, Mexico

<sup>4</sup> UMDI-Juriquilla, Facultad de Ciencias, Universidad Nacional Autónoma de México, Querétaro, Mexico

<sup>5</sup> Departments of Physics, University of Nevada Reno, Reno, USA

<sup>6</sup> Facultad de Ciencias, Universidad Nacional Autónoma de México, Ciudad de México, Mexico